Geosci. Model Dev. Discuss., 6, 5801–5862, 2013
www.geosci-model-dev-discuss.net/6/5801/2013/
doi:10.5194/gmdd-6-5801-2013

Geoscientific Model Development Discussions
Open Access

An orthogonal curvilinear terrain-following coordinate for atmospheric models

Y. Li[1], **B. Wang**[1,2], **and D. Wang**[3]

[1]State Key Laboratory of Numerical Modeling for Atmospheric Sciences and Geophysical Fluid Dynamics, Institute of Atmospheric Physics, Chinese Academy of Sciences, Beijing, China
[2]Ministry of Education Key Laboratory for Earth System Modeling, and Center for Earth System Science, Tsinghua University, Beijing, China
[3]State Key Laboratory of Severe Weather, Chinese Academy of Meteorological Sciences, Beijing, China

Received: 27 September 2013 – Accepted: 29 October 2013 – Published: 27 November 2013

Correspondence to: Y. Li (liyiyuan@mail.iap.ac.cn)

Published by Copernicus Publications on behalf of the European Geosciences Union.

Abstract

We have designed an orthogonal curvilinear terrain-following coordinate (the orthogonal σ coordinate, or the OS coordinate) to overcome two well-known problems in the classic σ coordinate, namely, pressure gradient force (PGF) errors and advection errors. First, in the design of basis vectors, we rotate the basis vectors of the z coordinate in a particular way in order to reduce the PGF errors and add a special rotation parameter b to each rotation angel in order to reduce the advection errors. Second, the corresponding definition of each OS coordinate is solved through its basis vectors. Third, the scalar equations of the OS coordinate are solved by expanding the vector equation using the basis vectors. Since the computational form of PGF has only one term in each momentum equation of the OS coordinate, the PGF errors will be significantly reduced, according to Li et al. (2012). When a proper b is chosen, the σ levels over a steep terrain can be significantly smoothed, therefore alleviating the advection errors in the OS coordinate. This is demonstrated by a series of 2-D linear advection experiments under a unified framework.

1 Introduction

The complex surface of the Earth is the lower boundary for numerical models, which have become more and more important for operational forecast and scientific research. There are mainly two kinds of methods to tackle the terrain in a model: using a proper vertical coordinate, such as the terrain-following coordinate proposed by Phillips (1957), or using the cut-cell method that has been used in the computational fluid dynamics and recently been developed by many researchers for simulating atmospheric and oceanic flows over irregular geometry (Adcroft et al., 1997; Yamazaki and Satomura, 2010; Adcroft, 2013; Steppeler et al., 2013). Until now, the terrain-following coordinate is the most popular choice for the atmospheric and oceanic models; for example, the grid-point atmospheric model of IAP LASG, GAMIL (Wang

GMDD
6, 5801–5862, 2013

et al., 2004); the Met Office's unified model, MetUM (Davies et al., 2005); the weather research and forecasting modeling system, WRF (Skamarock et al., 2008); the consortium for small-scale modelling, COSMO (Schättler et al., 2012); the model for prediction across scales, MPAS (Skamarock et al., 2012); the hybrid coordinate ocean model, HYCOM (Bleck, 2002; Wallcraft et al., 2009); and the nucleus for European modelling of the ocean, NEMO (Madec, 2008).

The terrain-following coordinate (σ coordinate) can be classified into two types: the pressure-based σ coordinate originated by Phillips (1957), and the height-based σ coordinate first designed by Gal-Chen and Somerville (1975). Both types are non-orthogonal coordinates, in which the σ coordinate levels are non-horizontal, and the computational form of pressure gradient force (PGF) has two terms (Zängl, 2002; Steppeler et al., 2003; Li et al., 2011, 2012; Siddorn and Furner, 2013). For these σ coordinate models, there are two well-known computational errors near a steep terrain (Sangster, 1960; Smagorinsky et al., 1967; Sundquist, 1975, 1976; Janjić, 1977; Mesinger, 1982; Haney, 1991; Konor and Arakawa, 1997; Ji et al., 2005; Mesinger, et al., 2012): the PGF errors and the advection errors.

So far, the two errors have been tackled separately. To overcome the PGF errors, methods have been designed based on the classic σ coordinate. Most of them tried to alleviate the PGF errors to an acceptable level, but kept on using two terms for the PGF in the σ coordinate (Corby et al., 1972; Gary, 1973; Qian and Zhong, 1986; Blumberg and Mellor, 1987; Yu, 1989; Lin et al., 1997; Adcroft et al., 2008; Sikirić et al., 2009; Berntsen, 2011; Bradley and Dowling, 2012). Alternatively, Li et al. (2012) proposed to use the covariant scalar equations of the σ coordinate in a numerical model, which can keep the computational form of PGF as one term in the σ coordinate as in the z coordinate, so as to reduce the PGF errors significantly. However, there are additional terms in their equations associated with the non-orthogonal characteristic of the σ coordinate, which may potentially cause numerical problems. In conclusion, all these efforts have been done in the non-orthogonal σ coordinate.

GMDD
6, 5801–5862, 2013

For the advection errors, methods were mostly designed to smooth the σ coordinate levels above the steep terrain to decrease the advection errors. A common method is the hybrid vertical coordinate used in many numerical models (Arakawa and Lamb, 1977; Simmons and Burridge, 1981; Simmons and Strüfing 1983). More recently, Schär et al. (2002) proposed a new smooth level vertical coordinate (SLEVE), which is a height-based coordinate to smooth the σ coordinate levels above a complex terrain and has been implemented in the COSMO model. Zängl (2003) developed the SLEVE into a pressure-based coordinate, and Leuenberger (2010) generalized it into more practicable form. Lately, a smooth terrain-following (STF) coordinate was proposed, which can smooth the σ levels much more than the SLEVE and has been implemented in the MPAS model (Klemp, 2011, 2012). Note that all these methods have been successful at alleviating the advection errors in the σ coordinate via smoothing the σ coordinate levels above a steep terrain; however, they did not consider handling the "PGF errors" at the same time.

In this study, we aim to deal with the two well-known computational errors of the classic σ coordinate (CS coordinate) together, through designing an orthogonal curvilinear terrain-following coordinate (OS coordinate) in a unique way. First, we take "reversed" steps from those of the CS coordinate, which is to solve the basis vectors of this new coordinate first and then the definition of every coordinate. Based on the basis vectors of the OS coordinate, we solve its scalar equations. Then, a unified framework is proposed to combine the z coordinate, the CS coordinate, and the OS coordinate. Finally, a series of idealized advection experiments are tested using this unified framework to exam the performance of the CS coordinate and OS coordinate in terms of advection errors.

2 The orthogonal curvilinear terrain-following coordinate

The basic principle of designing a terrain-following coordinate is to turn the surface of the Earth into a coordinate surface, therefore simplifying the lower boundary condition

GMDD
6, 5801–5862, 2013

in a numerical model. When designing a CS coordinate, researchers first designed the expression of the vertical coordinate in order to turn the terrain into a sigma level, as in Phillips (1957) and Gal-Chen and Somerville (1975), and then solved the basis vectors of the CS coordinate (black arrows in Fig. 1). However, we take an opposite approach. First, we solve the basis vectors of the OS coordinate, which are terrain-following and orthogonal, and then use the definitions of these basis vectors to solve the expression of every coordinate of the OS coordinate (green arrows in Fig. 1).

All the principles of the basis vectors and the OS coordinate are summarized in Table 1. In the following sub-sections, we first solve the basis vectors of the OS coordinate and the definition of each coordinate. Then, we demonstrate the basic characteristics of the OS coordinate.

2.1 The basis vectors

In order to achieve the requirements of the basis vectors described in Table 1, we use a special coordinate rotation to obtain the basis vectors of the OS coordinate, which is orthogonal and terrain-following. Specifically, we rotate the basis vectors of the z coordinate until its z axis is in line with the normal vector of the terrain, and a 2-D schematic of this rotation is shown in Fig. 2. In a 3-D rotation, we view it as a combination of two sets of 2-D rotation revolved around the coordinate axes, which will be illustrated later.

Since the basis vectors of the z coordinate are orthogonal, and the rotations revolved around the coordinate axes are orthogonal transformation, which keeps the original characteristics of the basis vectors, the rotated basis vectors are orthogonal. On the other hand, the z axis of the rotated basis vector is in line with the normal vector of the terrain, so the x axis and y axis of the rotated basis vectors are in the tangent plane of the terrain, which means the rotated basis vectors are terrain-following. In conclusion, the rotated basis vectors are both orthogonal and terrain-following.

In a 3-D system, there are four kinds of rotations to solve the basis vectors of the OS coordinate. Here, we use one of them as an example; the other three will be

GMDD
6, 5801–5862, 2013

introduced in Appendix A. First, we rotate the basis vectors of the z coordinate (the black arrows in Fig. 3) around its y axis until its z axis is in line with the projection of the normal vector of the terrain on the plane Oxz (the burgundy dash-dotted line), then we obtain the coordinate system $[O;\boldsymbol{x}_1,\boldsymbol{y}_1,\boldsymbol{z}_1]$, which is drawn as the blue arrows in Fig. 3. Second, we rotate the coordinate $[O;\boldsymbol{x}_1,\boldsymbol{y}_1,\boldsymbol{z}_1]$ around its $\boldsymbol{x}_1$ axis until the $\boldsymbol{z}_1$ axis is in line with the normal vector of the terrain (the burgundy arrow in Fig. 3), and then we obtain a coordinate system $[O;\boldsymbol{x}_2,\boldsymbol{y}_2,\boldsymbol{z}_2]$, which has a set of orthogonal and terrain-following basis vectors. Finally, using the two rotation angels θ' and λ' shown in Fig. 3, we can solve the expression of these basis vectors.

Here, we solve the basis vectors expressed by the rotation angels $\theta'$and λ'in a 3-D rotation. The relationship between the original basis vectors and the rotated ones are given by

$$\begin{pmatrix} \boldsymbol{i}' \\ \boldsymbol{j}' \\ \boldsymbol{k}' \end{pmatrix} = \begin{pmatrix} \cos\alpha_1 \cos\beta_1 \cos\gamma_1 \\ \cos\alpha_2 \cos\beta_2 \cos\gamma_2 \\ \cos\alpha_3 \cos\beta_3 \cos\gamma_3 \end{pmatrix} \begin{pmatrix} \boldsymbol{i} \\ \boldsymbol{j} \\ \boldsymbol{k} \end{pmatrix}, \tag{1}$$

where $\boldsymbol{i}$, $\boldsymbol{j}$, and $\boldsymbol{k}$ are the basis vectors of the original coordinate, $\boldsymbol{i}'$, $\boldsymbol{j}'$, and $\boldsymbol{k}'$ are the basis vectors of the rotated coordinate, and α_i, β_i, and γ_i (i = 1,2, and 3) are the angels between the original x, y, and z axis and the corresponding rotated x', y', and z' axis. Using the space geometry, we solve the rotation angels in the first rotation shown in Fig. 3 as follows:

$$\begin{pmatrix} \alpha_1 \beta_1 \gamma_1 \\ \alpha_2 \beta_2 \gamma_2 \\ \alpha_3 \beta_3 \gamma_3 \end{pmatrix} = \begin{pmatrix} \theta' & \frac{\pi}{2} & \frac{\pi}{2} - \theta' \\ \frac{\pi}{2} & 0 & \frac{\pi}{2} \\ \frac{\pi}{2} + \theta' & \frac{\pi}{2} & \theta' \end{pmatrix}, \tag{2}$$

GMDD
6, 5801–5862, 2013

then we substitute Eq. (2) into Eq. (1) to obtain the basis vectors of the coordinate $[O; \boldsymbol{x}_1, \boldsymbol{y}_1, z_1]$ as follows:

$$\begin{pmatrix} \boldsymbol{x}_1 \\ \boldsymbol{y}_1 \\ z_1 \end{pmatrix} = \begin{pmatrix} \cos\theta' & 0 & \sin\theta' \\ 0 & 1 & 0 \\ -\sin\theta' & 0 & \cos\theta' \end{pmatrix} \begin{pmatrix} \boldsymbol{i} \\ \boldsymbol{j} \\ \boldsymbol{k} \end{pmatrix}. \tag{3}$$

Using the same way, we solve the rotation angels of the second rotation shown in Fig. 3 as follows:

$$\begin{pmatrix} \alpha_1 & \beta_1 & \gamma_1 \\ \alpha_2 & \beta_2 & \gamma_2 \\ \alpha_3 & \beta_3 & \gamma_3 \end{pmatrix} = \begin{pmatrix} 0 & \frac{\pi}{2} & \frac{\pi}{2} \\ \frac{\pi}{2} & \lambda' & \frac{\pi}{2} - \lambda' \\ \frac{\pi}{2} & \frac{\pi}{2} + \lambda' & \lambda' \end{pmatrix}, \tag{4}$$

and through substituting Eq. (4) into Eq. (1), we solve the expression of the basis vectors of the coordinate $[O; \boldsymbol{x}_2, \boldsymbol{y}_2, z_2]$,

$$\begin{pmatrix} \boldsymbol{x}_2 \\ \boldsymbol{y}_2 \\ z_2 \end{pmatrix} = \begin{pmatrix} 1 & 0 & 0 \\ 0 & \cos\lambda' & \sin\lambda' \\ 0 & -\sin\lambda' & \cos\lambda' \end{pmatrix} \begin{pmatrix} \boldsymbol{x}_1 \\ \boldsymbol{y}_1 \\ z_1 \end{pmatrix}. \tag{5}$$

Finally, we substitute Eq. (3) into Eq. (5) to solve the rotated basis vectors as follows:

$$\begin{pmatrix} \boldsymbol{x}_2 \\ \boldsymbol{y}_2 \\ z_2 \end{pmatrix} = \begin{pmatrix} \cos\theta' & 0 & \sin\theta' \\ -\sin\lambda'\sin\theta' & \cos\lambda' & \sin\lambda'\cos\theta' \\ -\cos\lambda'\sin\theta' & -\sin\lambda' & \cos\lambda'\cos\theta' \end{pmatrix} \begin{pmatrix} \boldsymbol{i} \\ \boldsymbol{j} \\ \boldsymbol{k} \end{pmatrix}, \tag{6}$$

where $\cos\theta' = \frac{1}{\sqrt{\left(\frac{\partial h}{\partial x}\right)^2 + 1}}$, $\cos\lambda' = \frac{\sqrt{\left(\frac{\partial h}{\partial x}\right)^2 + 1}}{\sqrt{\left(\frac{\partial h}{\partial x}\right)^2 + \left(\frac{\partial h}{\partial y}\right)^2 + 1}}$, and $h = h(x, y)$ represents the terrain.

The expressions of the basis vectors solved by all four kinds of 3-D rotations can be summarized into two sets (Table 2). Note that, since the horizontal components of

GMDD
6, 5801–5862, 2013

these two sets of basis vectors, $\boldsymbol{i}_o$ and $\boldsymbol{j}_o$, are in the tangent plane of the terrain, and their vertical components $\boldsymbol{k}_o$ are in line with the normal vector of the terrain, these two sets of basis vectors are both terrain-following vectors except for the different directions of their horizontal components ($\boldsymbol{i}_o$ and $\boldsymbol{j}_o$).

Finally, we design a rotation parameter b in order to make the horizontal components of the basis vectors more horizontal with increasing height and finally equal to the basis vectors of the z coordinate at the top of the model. There are three principles for this rotation parameter b: (1) it should be 1 on the surface of the terrain; (2) it should be 0 at the top of the model; and (3) it should monotonically decrease with increasing height z. Note that these three requirements of the rotation parameter b are exactly the same as those of defining the vertical coordinate of the CS coordinate, which means any existed definition for the vertical coordinate of the CS coordinate can be used as the rotation parameter b in the OS coordinate. Then, we add the rotation parameter b with every rotation angel in the basis vectors of Table 2, so the basis vectors of the OS coordinate are at last solved as in Table 3.

2.2 Definition of each coordinate

Since the definition of each coordinate is to clarify the "coordinate transformation" from one coordinate to the other, such as the definition of σ, we use a "cross-point way" to solve the coordinate transformation between the z coordinate and the OS coordinate, instead of directly defining each coordinate in the OS coordinate.

We use the expressions of the basis vectors of the OS coordinate in Table 3 to obtain the expression of each coordinate. First, let each coordinate of the OS coordinate be

$$x' = x'(x, y, z), \tag{7}$$

$$y' = y'(x, y, z), \tag{8}$$

$$\sigma = \sigma(x, y, z), \tag{9}$$

GMDD
6, 5801–5862, 2013

where x, y, and z are the coordinates of the z coordinate, x', y', and σ are the coordinates of the OS coordinate. Since the OS coordinate is orthogonal, namely, its covariant and contravariant basis vectors are the same, we use the contravariant basis vectors as an example. These definitions are given as follows:

$$\boldsymbol{e}^1 = \frac{\partial x'}{\partial x}\boldsymbol{i} + \frac{\partial x'}{\partial y}\boldsymbol{j} + \frac{\partial x'}{\partial z}\boldsymbol{k}, \tag{10}$$

$$\boldsymbol{e}^2 = \frac{\partial y'}{\partial x}\boldsymbol{i} + \frac{\partial y'}{\partial y}\boldsymbol{j} + \frac{\partial y'}{\partial z}\boldsymbol{k}, \tag{11}$$

$$\boldsymbol{e}^3 = \frac{\partial \sigma}{\partial x}\boldsymbol{i} + \frac{\partial \sigma}{\partial y}\boldsymbol{j} + \frac{\partial \sigma}{\partial z}\boldsymbol{k}. \tag{12}$$

By comparing Eqs. (10)–(12) with the expressions of the basis vectors of the OS coordinate in Table 3, we can obtain the partial differential equations (PDEs) of each coordinate of the OS coordinate. Then solving these PDEs, we obtain the expression of each coordinate of the OS coordinate.

Since solving these PDEs of each coordinate of the OS coordinate is complex, we use an alternative way to define the coordinate transformation from the z coordinate to the OS coordinate, namely, to solve the coordinate values at a grid point using the OS coordinate and then solve them again using the z coordinate. We call this the "cross-point way," which is mentioned at the beginning of Sect. 2.2. In the following computations, we use the second kind of basis vectors of the OS coordinate in Table 3 as an example to elucidate how to carry out this coordinate transformation.

First, comparing Eqs. (10)–(12) with the second kind of basis vectors of the OS coordinate in Table 3, we obtain the PDEs of each coordinates as follows:

GMDD
6, 5801–5862, 2013

the horizontal coordinate x' of the OS coordinate,

$$\frac{\partial x'}{\partial x} = \cos(b \cdot \theta'), \tag{13}$$

$$\frac{\partial x'}{\partial y} = 0, \tag{14}$$

$$\frac{\partial x'}{\partial z} = \sin(b \cdot \theta'); \tag{15}$$

the horizontal coordinate y' of the OS coordinate,

$$\frac{\partial y'}{\partial x} = -\sin(b \cdot \theta') \cdot \sin(b \cdot \lambda'), \tag{16}$$

$$\frac{\partial y'}{\partial y} = \cos(b \cdot \lambda'), \tag{17}$$

$$\frac{\partial y'}{\partial z} = \cos(b \cdot \theta') \cdot \sin(b \cdot \lambda'); \tag{18}$$

the vertical coordinate σ of the OS coordinate,

$$\frac{\partial \sigma}{\partial x} = -\sin(b \cdot \theta') \cdot \cos(b \cdot \lambda'), \tag{19}$$

$$\frac{\partial \sigma}{\partial y} = -\sin(b \cdot \lambda'), \tag{20}$$

$$\frac{\partial \sigma}{\partial z} = \cos(b \cdot \theta') \cdot \cos(b \cdot \lambda'). \tag{21}$$

Solving these three sets of PDEs separately, we can obtain explicit expressions of x', y', and σ of the OS coordinate. For simplicity, we solve the coordinates of the OS coordinate in 2-D, so the PDEs of coordinate x' and σ are transformed into the

GMDD
6, 5801–5862, 2013

ordinary differential equations (ODEs) as follows:
the coordinate x',

$$\frac{\mathrm{d}z}{\mathrm{d}x} = -\cot(b\cdot\theta'); \tag{22}$$

the coordinate σ,

$$\frac{\mathrm{d}z}{\mathrm{d}x} = \tan(b\cdot\theta'). \tag{23}$$

Because the explicit solution of ODEs of Eqs. (22) and (23) is complex, we solve their numerical solution instead, and then we obtain the pattern of the x' and σ coordinate lines shown in Fig. 4. Since the resolution of the x' coordinate is high near the top of the terrain as shown in Fig. 4, the Courant–Friedrichs–Lewy (CFL) criterion should be considered in the design of the x' coordinate, which needs to be dealt with by further experiments.

Using these coordinate lines shown in Fig. 4, we then calculate the coordinate of every cross point in the z coordinate and the OS coordinate, respectively, which is exactly the coordinate transformation between the z coordinate and the OS coordinate (Fig. 5). Specifically, the coordinate of every cross point is valued as (x_1, z_1) in the z coordinate, while the coordinate value of this point in the OS coordinate is (b_1, a_1), for the value of each coordinate line is its coordinate in the OS coordinate.

Finally, through the cross-point way illustrated in Fig. 5, the coordinate transformation between the z coordinate and the OS coordinate is obtained (Fig. 6). Moreover, the coordinate transformation of the OS coordinate preserves three benefits of the classic σ coordinate: (1) the points on the terrain in the z coordinate (open black circles in the bottom of Fig. 6) are transformed into the points with their vertical coordinate being zero in the OS coordinate (solid red squares in the bottom of Fig. 6); (2) when there is non-terrain and at the top of the model, the points in the OS coordinate are those in the z coordinate; (3) the irregular physical space (open black circles in Fig. 6) is transformed into a regular computational grid in the OS coordinate (solid red squares in Fig. 6).

GMDD
6, 5801–5862, 2013

2.3 Basic characteristics

First, we use the $\mathbf{g}_{ij}$ and the matrix of the coordinate transformation to testify the orthogonality of the OS coordinate. Then, via solving the expression of the basis vectors on the terrain, we verify the basis vectors of the OS coordinate are terrain-following. Finally, we use three examples to demonstrate the ability of rotation parameter b to smooth the σ levels above a steep terrain.

Since the definition of $\mathbf{g}_{ij}$ is given by

$$\mathbf{g}_{ij} = \begin{pmatrix} \boldsymbol{e}_1 \cdot \boldsymbol{e}_1 & \boldsymbol{e}_1 \cdot \boldsymbol{e}_2 & \boldsymbol{e}_1 \cdot \boldsymbol{e}_3 \\ \boldsymbol{e}_2 \cdot \boldsymbol{e}_1 & \boldsymbol{e}_2 \cdot \boldsymbol{e}_2 & \boldsymbol{e}_2 \cdot \boldsymbol{e}_3 \\ \boldsymbol{e}_3 \cdot \boldsymbol{e}_1 & \boldsymbol{e}_3 \cdot \boldsymbol{e}_2 & \boldsymbol{e}_3 \cdot \boldsymbol{e}_3 \end{pmatrix}, \tag{24}$$

where $\boldsymbol{e}_i$ ($i = 1, 2$, and 3) are the basis vectors of a coordinate, we calculate $\mathbf{g}_{ij}$ of the OS coordinate using its basis vectors listed in Table 3,

$$\mathbf{g}_{ij} = \begin{pmatrix} 1 & 0 & 0 \\ 0 & 1 & 0 \\ 0 & 0 & 1 \end{pmatrix}. \tag{25}$$

Equation (25) manifests that the basis vectors of the OS coordinate are orthogonal and unit vectors. Furthermore, we transform the expressions of the basis vectors of the OS coordinate in Table 3 into a matrix:

the first kind of the basis vectors

$$\begin{pmatrix} \boldsymbol{i}_o \\ \boldsymbol{j}_o \\ \boldsymbol{k}_o \end{pmatrix} = \begin{pmatrix} \cos(b\cdot\lambda) & -\sin(b\cdot\theta)\sin(b\cdot\lambda) & -\cos(b\cdot\theta)\sin(b\cdot\lambda) \\ 0 & \cos(b\cdot\theta) & -\sin(b\cdot\theta) \\ \sin(b\cdot\lambda) & \sin(b\cdot\theta)\cos(b\cdot\lambda) & \cos(b\cdot\theta)\cos(b\cdot\lambda) \end{pmatrix} \begin{pmatrix} \boldsymbol{i} \\ \boldsymbol{j} \\ \boldsymbol{k} \end{pmatrix}, \tag{26}$$

the second kind of the basis vectors

$$\begin{pmatrix} \boldsymbol{i}_o \\ \boldsymbol{j}_o \\ \boldsymbol{k}_o \end{pmatrix} = \begin{pmatrix} \cos\left(b\cdot\theta'\right) & 0 & \sin\left(b\cdot\theta'\right) \\ -\sin\left(b\cdot\theta'\right)\sin\left(b\cdot\lambda'\right) & \cos\left(b\cdot\lambda'\right) & \cos\left(b\cdot\theta'\right)\sin\left(b\cdot\lambda'\right) \\ -\sin\left(b\cdot\theta'\right)\cos\left(b\cdot\lambda'\right) & -\sin\left(b\cdot\lambda'\right) & \cos\left(b\cdot\theta'\right)\cos\left(b\cdot\lambda'\right) \end{pmatrix} \begin{pmatrix} \boldsymbol{i} \\ \boldsymbol{j} \\ \boldsymbol{k} \end{pmatrix}. \tag{27}$$

GMDD
6, 5801–5862, 2013

The matrixes on the right hand side (RHS) of Eqs. (26) and (27) are called the transformation matrixes, which demonstrate the relationship between the transformed coordinate and the original one. Then, we calculate the determinant of these two transformation matrixes as follows:

the first kind of the basis vectors

$$\begin{vmatrix} \cos(b\cdot\lambda) & -\sin(b\cdot\lambda)\sin(b\cdot\theta) & -\sin(b\cdot\lambda)\cos(b\cdot\theta) \\ 0 & \cos(b\cdot\theta) & -\sin(b\cdot\theta) \\ \sin(b\cdot\lambda) & \cos(b\cdot\lambda)\sin(b\cdot\theta) & \cos(b\cdot\lambda)\cos(b\cdot\theta) \end{vmatrix} = 1, \tag{28}$$

the second kind of the basis vectors

$$\begin{vmatrix} \cos\left(b\cdot\theta'\right) & 0 & \sin\left(b\cdot\theta'\right) \\ -\sin\left(b\cdot\lambda'\right)\sin\left(b\cdot\theta'\right) & \cos\left(b\cdot\lambda'\right) & \sin\left(b\cdot\lambda'\right)\cos\left(b\cdot\theta'\right) \\ -\cos\left(b\cdot\lambda'\right)\sin\left(b\cdot\theta'\right) & -\sin\left(b\cdot\lambda'\right) & \cos\left(b\cdot\lambda'\right)\cos\left(b\cdot\theta'\right) \end{vmatrix} = 1. \tag{29}$$

Equations (28) and (29) show that the transformation matrixes of the OS coordinate are orthogonal, namely, the associated coordinate transformation is "the orthogonal transformation of the first kind." So the basis vectors of the OS coordinate preserve the characteristics of the z coordinate, which means the basis vectors of the OS coordinate are orthogonal and unit vectors.

Next, via substituting $b = 1$ and every rotation angel into the expressions of the basis vectors in Table 3, we obtain the vertical component of the basis vectors of the OS coordinate on the terrain as follows:

$$\begin{aligned} \boldsymbol{k}_o &= \frac{-\frac{\partial h}{\partial x}}{\sqrt{\left(\frac{\partial h}{\partial x}\right)^2+\left(\frac{\partial h}{\partial y}\right)^2+1}}\boldsymbol{i} + \frac{-\frac{\partial h}{\partial y}}{\sqrt{\left(\frac{\partial h}{\partial x}\right)^2+\left(\frac{\partial h}{\partial y}\right)^2+1}}\boldsymbol{j} + \frac{1}{\sqrt{\left(\frac{\partial h}{\partial x}\right)^2+\left(\frac{\partial h}{\partial y}\right)^2+1}}\boldsymbol{k} \\ &= \frac{1}{\sqrt{\left(\frac{\partial h}{\partial x}\right)^2+\left(\frac{\partial h}{\partial y}\right)^2+1}}\left(-\frac{\partial h}{\partial x}\boldsymbol{i} - \frac{\partial h}{\partial y}\boldsymbol{j} + \boldsymbol{k}\right). \end{aligned} \tag{30}$$

GMDD
6, 5801–5862, 2013

Comparing Eq. (30) with the normal vector of a terrain given by Eq. (A1), we obtain that the vertical component of basis vectors of the OS coordinate is in line with the normal vector of the terrain. Since the basis vectors of the OS coordinate are orthogonal, its horizontal components are in the tangent plane of the terrain, namely, the basis vectors of the OS coordinate are terrain-following. In addition, when there is non-terrain, which means $h = 0$ and at the top of the model with $b = 0$, the expressions of the basis vectors of the OS coordinate in Table 3 become,

$$\boldsymbol{i}_o = \boldsymbol{i}, \tag{31}$$

$$\boldsymbol{j}_o = \boldsymbol{j}, \tag{32}$$

$$\boldsymbol{k}_o = \boldsymbol{k}. \tag{33}$$

Equations (31)–(33) manifest the basis vectors of the OS coordinate are exactly equal to those of the z coordinate when there is no terrain and at the top of the model.

The characteristics of the basis vectors of the OS coordinate can be concluded in three aspects as shown in Fig. 7: (1) unit and orthogonal vectors, (2) terrain-following vectors, and (3) equal to the basis vectors of the z coordinate when there is no terrain and at the top of the model.

Finally, we propose three definitions of rotation parameter b in the basis vectors of the OS coordinate to show its ability in smoothing the σ levels above a steep terrain. These definitions are given as follows:

Linear b (Br1),

$$b = \frac{H_t - z}{H_t - h}, \tag{34}$$

Squared b (Br2),

$$b = \left(\frac{H_t - z}{H_t - h}\right)^2, \tag{35}$$

GMDD
6, 5801–5862, 2013

Exponential b (Br3),

$$b = \frac{e^{2(H_t-h)}}{e^{2(H_t-h)}-1}\cdot e^{-(z-h)} + \frac{-1}{e^{2(H_t-h)}-1}\cdot e^{(z-h)}, \tag{36}$$

where H_t is the top of the model, and $h = h(x,y)$ represents the terrain. All these three definitions satisfy the requirements of rotation parameter b, but with increasing complexity in terms of vertical variation from Eq. (34) to Eq. (36).

Figure 8 shows the σ levels along with these three kinds of b used in the basis vectors of the OS coordinate. First, all the slopes of the σ levels in the OS coordinate (colored lines) are no more than those of the CS coordinate (black lines). Second, while the height z increases, the slopes of the σ levels using these three definitions decrease significantly from Br1 (red lines) to Br3 (green lines). Third, the lowest σ-level is right along the terrain in all three definitions of b.

In conclusion, we have verified that the basis vectors of the OS coordinate are unit, orthogonal, and terrain-following. Particularly, the rotation parameter b in the basis vectors of the OS coordinate can significantly smooth the σ levels above a steep terrain.

3 Equations solved in the OS coordinate

3.1 The scalar equations

Using the basis vectors of the OS coordinate to expand a vector equation, we can obtain the scalar equations of the OS coordinate. In the following calculations, we use the vector equation of the atmosphere as an example, to solve the momentum, mass, and heat equations in the OS coordinate.

First, we expand the vector form of the momentum equation,

$$\frac{\partial \boldsymbol{v}}{\partial t} + (\boldsymbol{v}\cdot\boldsymbol{\nabla})\boldsymbol{v} = -\frac{1}{\rho}\boldsymbol{\nabla}p - 2\boldsymbol{\Omega}\times\boldsymbol{v} + \boldsymbol{g}. \tag{37}$$

GMDD
6, 5801–5862, 2013

The left hand side (LHS) of Eq. (37) is transformed into

$$\frac{\partial \boldsymbol{v}}{\partial t} = \frac{\partial v_i}{\partial t}\boldsymbol{q}_i + v_i\frac{\partial \boldsymbol{q}_i}{\partial t} = \frac{\partial v_i}{\partial t}\boldsymbol{q}_i, \tag{38}$$

and

$$(\boldsymbol{v}\cdot\boldsymbol{\nabla})\boldsymbol{v} = (v_i\boldsymbol{q}_i\cdot\boldsymbol{\nabla})v_i\boldsymbol{q}_i = \left(v_i\cdot\frac{\partial}{\partial q^i}\right)v_i\boldsymbol{q}_i. \tag{39}$$

While the RHS of Eq. (37) is transformed as follows,

$$-\frac{1}{\rho}\boldsymbol{\nabla}p = -\frac{1}{\rho}\frac{\partial p}{\partial q^i}\boldsymbol{q}_i, \tag{40}$$

$$-2\boldsymbol{\Omega}\times\boldsymbol{v} = -2(\Omega_2 v_3 - \Omega_3 v_2)\boldsymbol{q}_1 - 2(-\Omega_1 v_3 + \Omega_3 v_1)\boldsymbol{q}_2 - 2(\Omega_1 v_2 - \Omega_2 v_1)\boldsymbol{q}_3, \tag{41}$$

and

$$\boldsymbol{g} = g_i\boldsymbol{q}_i. \tag{42}$$

Second, we expand the vector form of the mass equation,

$$\frac{\partial \rho}{\partial t} + \boldsymbol{\nabla}\cdot(\rho\boldsymbol{v}) = 0. \tag{43}$$

Only the second term on the LHS of Eq. (43) changes to

$$\boldsymbol{\nabla}\cdot(\rho\boldsymbol{v}) = \frac{1}{\sqrt{g}}\frac{\partial}{\partial q^i}\left(\sqrt{g}\rho v_i\right). \tag{44}$$

Via Eq. (25), we obtain $\sqrt{g} = 1$, and then Eq. (44) becomes

$$\boldsymbol{\nabla}\cdot(\rho\boldsymbol{v}) = \frac{\partial}{\partial q^i}(\rho v_i). \tag{45}$$

GMDD
6, 5801–5862, 2013

Third, the vector form of the heat equation is given by

$$\frac{\partial T}{\partial t} + \boldsymbol{v} \cdot \boldsymbol{\nabla} T - \frac{RT}{C_p p} \frac{\mathrm{d}p}{\mathrm{d}t} = \frac{Q}{C_p}. \tag{46}$$

The second term on the LHS of Eq. (46) becomes

$$\boldsymbol{v} \cdot \boldsymbol{\nabla} T = v_i \frac{\partial T}{\partial q^i}. \tag{47}$$

Now, the scalar equations of the OS coordinate can be solved as follows: the momentum equations,

$$\frac{\partial u_o}{\partial t} + u_o \frac{\partial u_o}{\partial x'} + v_o \frac{\partial u_o}{\partial y'} + w_o \frac{\partial u_o}{\partial \sigma} = -\frac{1}{\rho} \frac{\partial p}{\partial x'} - 2(\Omega_{o2} w_o - \Omega_{o3} v_o) + g_{o1}, \tag{48}$$

$$\frac{\partial v_o}{\partial t} + u_o \frac{\partial v_o}{\partial x'} + v_o \frac{\partial v_o}{\partial y'} + w_o \frac{\partial v_o}{\partial \sigma} = -\frac{1}{\rho} \frac{\partial p}{\partial y'} + 2(\Omega_{o1} w_o - \Omega_{o3} u_o) + g_{o2}, \tag{49}$$

$$\frac{\partial w_o}{\partial t} + u_o \frac{\partial w_o}{\partial x'} + v_o \frac{\partial w_o}{\partial y'} + w_o \frac{\partial w_o}{\partial \sigma} = -\frac{1}{\rho} \frac{\partial p}{\partial \sigma} - 2(\Omega_{o1} v_o - \Omega_{o2} u_o) + g_{o3}; \tag{50}$$

the mass equation,

$$\frac{\partial \rho}{\partial t} + \frac{\partial}{\partial x'}(\rho u_o) + \frac{\partial}{\partial y'}(\rho v_o) + \frac{\partial}{\partial \sigma}(\rho w_o) = 0; \tag{51}$$

the heat equation,

$$\frac{\partial T}{\partial t} + u_o \frac{\partial T}{\partial x'} + v_o \frac{\partial T}{\partial y'} + w_o \frac{\partial T}{\partial \sigma} - \frac{RT}{C_p p} \frac{\mathrm{d}p}{\mathrm{d}t} = \frac{Q}{C_p}; \tag{52}$$

and the equation of state,

$$p = \rho R T. \tag{53}$$

GMDD
6, 5801–5862, 2013

In Eqs. (48)–(53), the parameters with subscript o are the scalars in the OS coordinate, which should be solved following the procedure described in Appendix B.

Note that the expression of the PGF in all three momentum equations, Eqs. (48)–(50), has only one term, which means the OS coordinate will significantly reduce the PGF errors, as suggested by Li et al. (2012) in their new method of implementing the classic σ coordinate. More importantly, the forms of the momentum equations in the OS coordinate are as simple as those in the z coordinate, which do not have the additional terms, such as the curvature terms existed in the equations of Li et al. (2012), therefore avoiding the potential numerical problems all together. However, the effect of the components of gravity in each momentum equation of the OS coordinate still needs to be investigated using more numerical experiments.

3.2 A unified framework

To show a way of implementing the OS coordinate in a numerical model, we first propose a unified framework to combine the equations in the z coordinate, the CS coordinate, and the OS coordinate. And there are two aspects to deal with these equation sets, "the difference in form" and "the difference in value." We set corresponding parameters to unify the different forms, and then separately define the different values of scalars in the three coordinates.

GMDD
6, 5801–5862, 2013

The unified equations of this framework are written as follows:

$$\frac{\partial u}{\partial t}+u\frac{\partial u}{\partial q^1}+v\frac{\partial u}{\partial q^2}+w\frac{\partial u}{\partial q^3}+\lambda_{11}=-\frac{1}{\rho}\delta_{1i}\frac{\partial p}{\partial q^i}-2\lambda_2\left(\Omega_2 w-\Omega_3 v\right)+g_1, \tag{54}$$

$$\frac{\partial v}{\partial t}+u\frac{\partial v}{\partial q^1}+v\frac{\partial v}{\partial q^2}+w\frac{\partial v}{\partial q^3}+\lambda_{12}=-\frac{1}{\rho}\delta_{2i}\frac{\partial p}{\partial q^i}+2\lambda_2\left(\Omega_1 w-\Omega_3 u\right)+g_2, \tag{55}$$

$$\frac{\partial w}{\partial t}+u\frac{\partial w}{\partial q^1}+v\frac{\partial w}{\partial q^2}+w\frac{\partial w}{\partial q^3}+\lambda_{13}=-\frac{1}{\rho}\delta_{3i}\frac{\partial p}{\partial q^i}-2\lambda_2\left(\Omega_1 v-\Omega_2 u\right)+g_3, \tag{56}$$

$$\frac{\partial \rho}{\partial t}+\frac{1}{\lambda_2}\frac{\partial}{\partial q^1}\left(\lambda_2\rho u\right)+\frac{1}{\lambda_2}\frac{\partial}{\partial q^2}\left(\lambda_2\rho v\right)+\frac{1}{\lambda_2}\frac{\partial}{\partial q^3}\left(\lambda_2\rho w\right)=0, \tag{57}$$

$$\frac{\partial T}{\partial t}+u\frac{\partial T}{\partial q^1}+v\frac{\partial T}{\partial q^2}+w\frac{\partial T}{\partial q^3}-\frac{RT}{C_p p}\frac{\mathrm{d}p}{\mathrm{d}t}=\frac{Q}{C_p}, \tag{58}$$

$$p=\rho RT. \tag{59}$$

where, i sums from 1 to 3, q^i are the coordinates, the values of λ_{im}, λ_2, and δ_{mi} (m = 1,2, and 3) are listed in the Table C1 of Appendix C. The scalars in Eqs. (54)–(59) represent their values in different coordinates, such as the scalars of velocity u, v, and w, the scalars of angular velocity Ω_m, and the scalars of gravity g_m, which should be solved separately in each coordinate using the corresponding matrix $\mathbf{t}_{ij}$ proposed in Appendix C.

In conclusion, through defining different values of the parameters in each coordinate as in Table C1 and choosing the different coordinate transformation matrix $\mathbf{t}_{ij}$ described in Appendix C, we can obtain the unified equations of the z coordinate, the CS coordinate, and the OS coordinate. Moreover, the equations of each coordinate can be conveniently switched from one to the other in this unified framework.

GMDD
6, 5801–5862, 2013

4 Idealized experiments used to compare advection errors

In order to examine the ability of the OS coordinate at handling the advection errors of the CS coordinate, we use the unified framework proposed in Sect. 3.2 to implement a series of 2-D idealized advection experiments. First, we make a basic comparison of the advection errors between the CS coordinate and the OS coordinate using an experiment of fixed spatial resolution. Then, we carry out sensitive experiments using various horizontal and vertical resolutions to investigate the variation of the advection errors in both coordinates.

4.1 Parameters of the 2-D advection experiments

Since the contravariant equations of the CS coordinate are the equations commonly used in many numerical models, in the following experiments we only make comparisons of the advection errors between the OS coordinate and the CS coordinate using the contravariant equations. Here we use the definition of σ as $\sigma = H_t \frac{z-h}{H_t-h}$, which was proposed by Gal-Chen and Somerville (1975). In addition, in the OS coordinate we choose its second kind of basis vectors as an example in the following computation. The expressions of the velocities in these two coordinates are respectively given as follows:

the CS coordinate using the covariant basis vectors,

$$\left(u'\ w'\right) = \left(u\ w\right)\begin{pmatrix} 1 & \frac{H_t-z}{H_t-h}\cdot\frac{\partial h}{\partial x} \\ 0 & \frac{H_t-h}{H_t} \end{pmatrix}^{-1} = \left(u\ w\right)\begin{pmatrix} 1 & H_t\cdot\frac{z-H_t}{(H_t-h)^2}\cdot\frac{\partial h}{\partial x} \\ 0 & \frac{H_t}{H_t-h} \end{pmatrix}, \tag{60}$$

the OS coordinate using the second kind of basis vectors,

$$\left(u'\ w'\right) = \left(u\ w\right)\begin{pmatrix} \cos\left(b\cdot\theta'\right) & \sin\left(b\cdot\theta'\right) \\ -\sin\left(b\cdot\theta'\right) & \cos\left(b\cdot\theta'\right) \end{pmatrix}^{-1} = \left(u\ w\right)\begin{pmatrix} \cos\left(b\cdot\theta'\right) & -\sin\left(b\cdot\theta'\right) \\ \sin\left(b\cdot\theta'\right) & \cos\left(b\cdot\theta'\right) \end{pmatrix}. \tag{61}$$

GMDD
6, 5801–5862, 2013

The linear advection equation is used in all the experiments,

$$\frac{\partial q}{\partial t} + u' \frac{\partial q}{\partial X} + w' \frac{\partial q}{\partial Z} = 0, \tag{62}$$

where q represents the anomaly field, u' and w' are the velocity components in the unified framework, and X and Z are the horizontal and vertical coordinates in the unified framework. Note that in the CS coordinate, the coordinates are solved by the definitions of x' and σ, while in the OS coordinate, the coordinates are calculated following the coordinate transformation illustrated in Figs. 5 and 6. Then, we discretize the advection Eq. (62) using the leapfrog scheme, so the discretization of Eq. (62) is written as follows:

$$\frac{q^{n+1}_{i,k} - q^{n-1}_{i,k}}{2\Delta t} + u' \frac{q^{n}_{i+1,k} - q^{n}_{i-1,k}}{2\Delta X} + w' \frac{q^{n}_{i,k+1} - q^{n}_{i,k-1}}{2\Delta Z} = 0. \tag{63}$$

And the periodic boundary condition is used in the horizontal, while the rigid-lid boundary condition is used in the vertical.

The other parameters of the 2-D advection experiments are shown in Fig. 9. In particular, the domain of the experiments is fixed with 0–300 m in the horizontal and 0–25 m in the vertical. And the definitions of the anomaly field q and the horizontal velocity u both follow the advection experiments designed by Schär et al. (2002). The expression of the anomaly field q is given by

$$q(x,z) = q_0 \cdot \begin{cases} \cos^2\left(\frac{\pi}{2} \cdot r\right), & r \le 1 \\ 0 \end{cases}, \tag{64}$$

GMDD
6, 5801–5862, 2013

where $q_0 = 1$, $r = \sqrt{\left(\frac{x-x_0}{A_x}\right)^2 + \left(\frac{z-z_0}{A_z}\right)^2}$, $x_0 = 100\,\mathrm{m}$, $z_0 = 9\,\mathrm{m}$, $A_x = 25\,\mathrm{m}$, and $A_z = 3\,\mathrm{m}$. The u field is given by

$$u(z) = u_0 \cdot \begin{cases} 1, & z_2 \le z \\ \sin^2\left(\frac{\pi}{2} \cdot \frac{z-z_1}{z_2-z_1}\right), & z_1 \le z \le z_2 \\ 0, & z \le z_1 \end{cases}, \tag{65}$$

where $u_0 = 1\,\mathrm{m\,s^{-1}}$, $z_1 = 4\,\mathrm{m}$, and $z_2 = 5\,\mathrm{m}$. Then, we use a bell-shaped terrain, which is a common choice in a theoretical analysis of airflow over a mountain, and the definition of it is given by

$$h(x) = H \cdot \frac{a^2}{(x - h_o)^2 + a^2}, \tag{66}$$

where $H = 3\,\mathrm{m}$, $h_o = 150\,\mathrm{m}$, and $a = 10\,\mathrm{m}$.

In each experiment, we integrate 400 time steps using the time step of $\mathrm{d}t = 0.25\,\mathrm{s}$. The horizontal and vertical resolutions in the transformed space are $\mathrm{d}X = 1\,\mathrm{m}$ and $\mathrm{d}Z = 0.5\,\mathrm{m}$, respectively, for the basic comparison as shown in Fig. 10a. For the sensitivity comparison, we use five different horizontal and vertical resolutions. Since in the OS coordinate we designed three different kinds of rotation parameter b, which are given by Eq. (34)–(36), we have four groups of experiments for the two coordinates, which are the CS coordinate and the OS coordinate with three different kinds of rotation parameter b. Here, we abbreviate all four groups of experiments as Cs, OsBr1, OsBr2, and OsBr3 correspondingly in the following comparison.

The computational grids in the basic comparison of the CS coordinate and the OS coordinate with three different rotation parameter b are shown in Fig. 10b–e. The horizontal Courant number in the CS coordinate is $\alpha_{\mathrm{cs}} = \frac{u \cdot \mathrm{d}t}{\mathrm{d}x} = 0.25$. Since the resolution of the x' coordinate is high near the top of the terrain in the OS coordinate as

GMDD
6, 5801–5862, 2013

shown in Fig. 10c–e, we calculate the minimum dx in OsBr1, OsBr2, and OsBr3, which are $dx = 0.5\,m$, $dx = 0.6\,m$, and $dx = 0.9\,m$. Then the maximum horizontal Courant numbers in the OsBr1, OsBr2, and OsBr3 are solved as follows: $\alpha_{osbr1} = \frac{u \cdot dt}{dx} = 0.5$, $\alpha_{osbr2} = \frac{u \cdot dt}{dx} = 0.42$, and $\alpha_{osbr3} = \frac{u \cdot dt}{dx} = 0.28$. In addition, we calculate the maximum vertical Courant numbers in the CS, OsBr1, OsBr2, and OsBr3 as follows: $\beta_{cs} = \frac{w' \cdot dt}{dZ} = 0.093$, $\beta_{osbr1} = \frac{w' \cdot dt}{dZ} = 0.084$, $\beta_{osbr2} = \frac{w' \cdot dt}{dZ} = 0.073$, $\beta_{osbr2} = \frac{w' \cdot dt}{dZ} = 0.008$. Note that, the more smoothing the σ levels become through the rotation parameter b, the lower the resolution of x' over the top of terrain in the OS coordinate is (Fig. 10c–e).

4.2 Basic comparison

Following Schär et al. (2002), we also calculate the absolute errors (AE) of the advection in the OS coordinate and the CS coordinate by comparing them with the results obtained from non-terrain simulations.

First, we compare the AE of both coordinates when the advection is over the top of the terrain (Fig. 11). Their patterns are similar; however, the maximum values of AE are significantly different. In particular, all the errors obtained by the three experiments of the OS coordinate (Fig. 11b–d) are much smaller than those in the CS coordinate (Fig. 11a). Note that the AE of OsBr3 (Fig. 11d) is two orders of magnitude smaller than those of the OS coordinate (Fig. 11a).

Then, we calculate the root mean square errors (RMSEs) of the advection in all the experiments at every time step (Fig. 12). The RMSEs of all the experiments using the OS coordinate (colored curves in Fig. 12) are consistently smaller than those in the CS coordinate, especially when using the exponential rotation parameters b (OsBr3; green), which is two orders of magnitude smaller than those in the CS coordinate at every time step.

GMDD
6, 5801–5862, 2013

4.3 Sensitive comparison of different spatial resolutions

Since the spatial resolution is an important factor in simulating the advection over terrain in the terrain-following coordinate (Schär et al., 2002), we use five different horizontal and vertical spatial resolutions listed in Table 4 to compare the variation of the advection errors between the CS coordinate and the OS coordinate. The maximum horizontal Courant number in the CS coordinate is $\alpha_{cs} = 0.5$, and the maximum horizontal Courant number in the OS coordinate is $\alpha_{osbr1} = 0.96$,which is calculated from the experiment of dX = 0.5 m in OsBr1. For each fixed-resolution experiment, we carry out four groups of experiments, which are Cs, OsBr1, OsBr2, and OsBr3; so there are a total of 32 groups (since four groups were implemented in the basic comparison in Sect. 4.2).

First, we compare the pattern of advection in both coordinates and use the results obtained by the experiment of dX = 8.0 m and dZ = 0.5 m as an example (Fig. 13). The results in the CS coordinate show large deformation, while the advection is over the top of the terrain as shown in the middle of Fig. 13a. However, using the OS coordinate with three kinds of rotation parameters, this deformation is alleviated, especially in the results obtained by OsBr3 (Fig. 13d).

Second, we calculate the RMSEs of the advection in both coordinates in all five different horizontal spatial resolutions at every time step (Fig. 14). Being consistent with the results obtained by the basic comparison (Fig. 12), the RMSEs in all the experiments using the OS coordinate (Fig. 14b–d) are smaller than those in the CS coordinate, especially the RMSE of OsBr3 (Fig. 14d); it is constantly two orders of magnitude smaller than those in the CS coordinate (Fig. 14a) in each experiment.

Next, we calculate the RMSEs obtained by using five different vertical spatial resolutions (Fig. 15). Again, the RMSEs in the OS coordinate (Fig. 15b–d) are smaller than those in the CS coordinate (Fig. 15a). Especially, the RMSE in OsBr3 (Fig. 15d) is constantly two orders of magnitude smaller than those in the CS coordinate (Fig. 15a).

GMDD
6, 5801–5862, 2013

Finally, we analyze the reason for the improvements of the OS coordinate via comparing the slopes of σ levels in the OS coordinate and the CS coordinate. The expression of the slopes of every σ levels in the CS coordinate are $\left(\frac{\partial z}{\partial x}\right)_\sigma = \frac{H_t - z}{H_t - h} \cdot \frac{\partial h}{\partial x}$ (Li et al., 2011), and those in the OS coordinate are given by $\left(\frac{\partial z}{\partial x}\right)_\sigma = \tan\left(b \cdot \arctan\left(\frac{\partial h}{\partial x}\right)\right)$. Here, we only calculate the slopes above $z = 4.0$ m, since the u field is zero below $z = 4.0$ m as expressed in Eq. (65). The slopes of σ levels above the top of terrain in the CS coordinate and OS coordinate are shown in Fig. 16, which is calculated by using the experiment of $dX = 2.0$ m and $dZ = 0.5$ m as an example.

Comparing with the RMSEs of the two sensitive experiments shown in Figs. 14 and 15, the values of the slopes show similar variation from the CS coordinate to the OS coordinate using three rotation parameters (Fig. 16). Specifically, all the values of the slopes in the OS coordinate are smaller than those in the CS coordinate; especially in the experiment of OsBr3, the values of the slopes are one order of magnitude smaller than those in the CS coordinate. In conclusion, through alleviating the slopes of the σ levels above the steep terrain, the OS coordinate significantly reduces the advection errors of the CS coordinate.

5 Conclusion and discussion

In order to overcome the two well known computational errors, the "PGF errors" and the "advection errors" in the classic σ coordinate together, an orthogonal curvilinear terrain-following coordinate that has a set of orthogonal and terrain-following basis vectors are proposed. The key is to use a very different approach to re-design a terrain-following coordinate. Since the OS coordinate is orthogonal, the computational form of PGF in each momentum equation has only one term so it will reduce the "PGF errors" significantly. Via designing a proper rotation parameter b in the OS coordinate, this new coordinate can conveniently smooth the σ levels, therefore significantly reducing the "advection errors" of the classic σ coordinate.

GMDD
6, 5801–5862, 2013

The design of the OS coordinate uses the opposite order from the design of the classic σ coordinate, which is to first construct the basis vectors and then the corresponding definition of each coordinate. Specifically, we rotate the basis vectors of the z coordinate until its vertical basis vector is in line with the normal vector of the terrain, and add a rotation parameter b to each rotation angle (Table 3), which make the new coordinate unit, orthogonal, and terrain-following (Fig. 7). Then, we use a "cross-point way" to solve the coordinate transformation between the z coordinate and the OS coordinate, instead of solving the explicit definition of each coordinate as commonly done. Furthermore, using the basis vectors of the OS coordinate to expand the vector equation, we solve the scalar equations of the OS coordinate; as a result, the computational form of PGF has only one term, therefore reducing the PGF errors, as illustrated in Li et al. (2012). Finally, based on the characteristics of the scalar equations of the OS coordinate, we design a unified framework to implement both the classic and the orthogonal σ coordinate using a set of unified equations, which is a facility for the application of this new coordinate in a numerical model.

Using this unified framework, we carried out a series of 2-D linear advection experiments to compare the advection errors of the two σ-coordinates associated with three different forms of rotation parameter b. First, in a basic comparison using the fixed resolution, the RMSEs in the OS coordinate are all smaller than those of the CS coordinate (Fig. 12). And then, in the sensitive experiments of increasing horizontal and vertical resolutions, the RMSEs in the OS coordinate are also much smaller than those of the CS coordinate (Figs. 14 and 15); especially when the OS coordinate uses the exponential rotation parameter b (Figs. 14d and 15d), the RMSEs are consistently two orders of magnitude smaller than those of the CS coordinate. Finally, we analyze the reason for the improvements of the OS coordinate and find that it is through alleviating the slopes of σ levels that the OS coordinate significantly reduces the advection errors of the CS coordinate.

Since the two well-known computational errors exist in both atmospheric and oceanic models that use the σ coordinate, the OS coordinate can be used for numerical

GMDD
6, 5801–5862, 2013

ocean models as well, potentially representing the dynamic effects of terrain more precisely and therefore simulating more realistic circulations near complex terrains. We understand that though the OS coordinate proposed in this study is theoretically sound, it may encounter some problems in practice, such as the effects of the component of gravity g_m in each momentum equation, and the CFL criterion above the steep terrain. Moreover, the effect of reduced advection errors by the OS coordinate should be compared with that by other methods, such as the hybrid σ coordinate, SLEVE and STF, and the comparison between the OS coordinate with the cut-cell method should be investigated by further experiments in terms of reducing the computational errors. The true benefits of the new coordinate need to be confirmed by more idealized and realistic experiments.

Appendix A

Coordinate rotations for solving the basis vectors of OS coordinate

There are four ways to rotate the basis vectors of the z coordinate to obtain the basis vectors of the OS coordinate. Specifically, there are two ways of rotations on the upslope and two on the downslope: (1) first rotation is around the x axis, and then around the rotated y axis, and (2) first rotation is around the y axis, and then around the rotated x axis. We introduced one way in Sect. 2, and now solve the expressions of the other three here.

First, we solve the expression on the upslope of the terrain as shown in Fig. A1. The normal vector of the terrain is the burgundy arrow in Fig. A1 and its expression is given by

$$\boldsymbol{l} = -\frac{\partial h}{\partial x}\boldsymbol{i} - \frac{\partial h}{\partial y}\boldsymbol{j} + \boldsymbol{k}, \tag{A1}$$

where $h = h(x, y)$ represents the terrain. On the upslope of the terrain, $\frac{\partial h}{\partial x} > 0$ and $\frac{\partial h}{\partial y} > 0$, while on the downslope of terrain, $\frac{\partial h}{\partial x} < 0$ and $\frac{\partial h}{\partial y} < 0$.

GMDD
6, 5801–5862, 2013

In this rotation, we first rotate the basis vectors of the z coordinate around the x axis and then the rotated y axis (the blue arrow y_1 shown in Fig. A1), and we get two rotation angels θ^* and λ^*.

Using the space geometry, we can solve the two rotation angels respectively as follows:

the first rotation,

$$\begin{pmatrix} \alpha_1 & \beta_1 & \gamma_1 \\ \alpha_2 & \beta_2 & \gamma_2 \\ \alpha_3 & \beta_3 & \gamma_3 \end{pmatrix} = \begin{pmatrix} 0 & \frac{\pi}{2} & \frac{\pi}{2} \\ \frac{\pi}{2} & \theta^* & \frac{\pi}{2} - \theta^* \\ \frac{\pi}{2} & \frac{\pi}{2} + \theta^* & \theta^* \end{pmatrix}; \tag{A2}$$

the second rotation,

$$\begin{pmatrix} \alpha_1 & \beta_1 & \gamma_1 \\ \alpha_2 & \beta_2 & \gamma_2 \\ \alpha_3 & \beta_3 & \gamma_3 \end{pmatrix} = \begin{pmatrix} \lambda^* & \frac{\pi}{2} & \frac{\pi}{2} - \lambda^* \\ \frac{\pi}{2} & 0 & \frac{\pi}{2} \\ \frac{\pi}{2} + \lambda^* & \frac{\pi}{2} & \lambda^* \end{pmatrix}, \tag{A3}$$

where $\cos\theta^* = \frac{1}{\sqrt{\left(\frac{\partial h}{\partial y}\right)^2 + 1}}$ and $\cos\lambda^* = \frac{\sqrt{\left(\frac{\partial h}{\partial y}\right)^2 + 1}}{\sqrt{\left(\frac{\partial h}{\partial x}\right)^2 + \left(\frac{\partial h}{\partial y}\right)^2 + 1}}$, substituting Eq. (A2) into Eq. (1), we get the basis vectors of the coordinate $[O; \boldsymbol{x}_1, \boldsymbol{y}_1, z_1]$ as follows:

$$\begin{pmatrix} \boldsymbol{x}_1 \\ \boldsymbol{y}_1 \\ z_1 \end{pmatrix} = \begin{pmatrix} 1 & 0 & 0 \\ 0 & \cos\theta^* & \sin\theta^* \\ 0 & -\sin\theta^* & \cos\theta^* \end{pmatrix} \begin{pmatrix} \boldsymbol{i} \\ \boldsymbol{j} \\ \boldsymbol{k} \end{pmatrix}. \tag{A4}$$

Substituting Eq. (A3) into Eq. (1), we obtain the basis vectors of the coordinate $[O; \boldsymbol{x}_2, \boldsymbol{y}_2, z_2]$ as follows:

$$\begin{pmatrix} \boldsymbol{x}_2 \\ \boldsymbol{y}_2 \\ z_2 \end{pmatrix} = \begin{pmatrix} \cos\lambda^* & 0 & \sin\lambda^* \\ 0 & 1 & 0 \\ -\sin\lambda^* & 0 & \cos\lambda^* \end{pmatrix} \begin{pmatrix} \boldsymbol{x}_1 \\ \boldsymbol{y}_1 \\ z_1 \end{pmatrix}. \tag{A5}$$

GMDD
6, 5801–5862, 2013

Finally, we substitute Eq. (A4) into Eq. (A5) to obtain the basis vectors of the coordinate $[O;\boldsymbol{x}_2,\boldsymbol{y}_2,\boldsymbol{z}_2]$, which is orthogonal and terrain-following and its expression is given by

$$\begin{pmatrix}\boldsymbol{x}_2\\ \boldsymbol{y}_2\\ \boldsymbol{z}_2\end{pmatrix}=\begin{pmatrix}\cos\lambda^* & -\sin\lambda^*\sin\theta^* & \sin\lambda^*\cos\theta^*\\ 0 & \cos\theta^* & \sin\theta^*\\ -\sin\lambda^* & -\cos\lambda^*\sin\theta^* & \cos\lambda^*\cos\theta^*\end{pmatrix}\begin{pmatrix}\boldsymbol{i}\\ \boldsymbol{j}\\ \boldsymbol{k}\end{pmatrix}. \tag{A6}$$

Second, we solve the expression of the basis vectors in the coordinate rotation on the downslope of the terrain. One of the rotations that is first around the x axis and then the rotated y axis is shown in Fig. A2.

The rotation angels in these two rotations are solved as follows:
the first rotation,

$$\begin{pmatrix}\alpha_1 & \beta_1 & \gamma_1\\ \alpha_2 & \beta_2 & \gamma_2\\ \alpha_3 & \beta_3 & \gamma_3\end{pmatrix}=\begin{pmatrix}0 & \frac{\pi}{2} & \frac{\pi}{2}\\ \frac{\pi}{2} & \theta & \frac{\pi}{2}+\theta\\ \frac{\pi}{2} & \frac{\pi}{2}-\theta & \theta\end{pmatrix}; \tag{A7}$$

the second rotation,

$$\begin{pmatrix}\alpha_1 & \beta_1 & \gamma_1\\ \alpha_2 & \beta_2 & \gamma_2\\ \alpha_3 & \beta_3 & \gamma_3\end{pmatrix}=\begin{pmatrix}\lambda & \frac{\pi}{2} & \frac{\pi}{2}+\lambda\\ \frac{\pi}{2} & 0 & \frac{\pi}{2}\\ \frac{\pi}{2}-\lambda & \frac{\pi}{2} & \lambda\end{pmatrix}, \tag{A8}$$

where $\cos\theta=\frac{1}{\sqrt{\left(\frac{\partial h}{\partial y}\right)^2+1}}$ and $\cos\lambda=\frac{\sqrt{\left(\frac{\partial h}{\partial y}\right)^2+1}}{\sqrt{\left(\frac{\partial h}{\partial x}\right)^2+\left(\frac{\partial h}{\partial y}\right)^2+1}}$. Using the same method of solving Eq. (A6), we can obtain the basis vectors of the coordinate $[O;\boldsymbol{x}_2,\boldsymbol{y}_2,\boldsymbol{z}_2]$, which is orthogonal and terrain-following and its expression is given by

$$\begin{pmatrix}\boldsymbol{x}_2\\ \boldsymbol{y}_2\\ \boldsymbol{z}_2\end{pmatrix}=\begin{pmatrix}\cos\lambda & -\sin\lambda\sin\theta & -\sin\lambda\cos\theta\\ 0 & \cos\theta & -\sin\theta\\ \sin\lambda & \cos\lambda\sin\theta & \cos\lambda\cos\theta\end{pmatrix}\begin{pmatrix}\boldsymbol{i}\\ \boldsymbol{j}\\ \boldsymbol{k}\end{pmatrix}. \tag{A9}$$

GMDD
6, 5801–5862, 2013

Finally, we solve the expression of the basis vectors in the coordinate rotation on the downslope of the terrain, which is first around the y axis and then the rotated x axis (Fig. A3).

The rotation angels in these two rotations are solved as follows:

the first rotation,

$$\begin{pmatrix} \alpha_1 & \beta_1 & \gamma_1 \\ \alpha_2 & \beta_2 & \gamma_2 \\ \alpha_3 & \beta_3 & \gamma_3 \end{pmatrix} = \begin{pmatrix} \theta^{\#} & \frac{\pi}{2} & \frac{\pi}{2}+\theta^{\#} \\ \frac{\pi}{2} & 0 & \frac{\pi}{2} \\ \frac{\pi}{2}-\theta^3 & \frac{\pi}{2} & \theta^{\#} \end{pmatrix}; \tag{A10}$$

the second rotation,

$$\begin{pmatrix} \alpha_1 & \beta_1 & \gamma_1 \\ \alpha_2 & \beta_2 & \gamma_2 \\ \alpha_3 & \beta_3 & \gamma_3 \end{pmatrix} = \begin{pmatrix} 0 & \frac{\pi}{2} & \frac{\pi}{2} \\ \frac{\pi}{2} & \lambda^{\#} & \frac{\pi}{2}+\lambda^{\#} \\ \frac{\pi}{2} & \frac{\pi}{2}-\lambda^{\#} & \lambda^{\#} \end{pmatrix}, \tag{A11}$$

where $\cos\theta^{\#} = \frac{1}{\sqrt{\left(\frac{\partial h}{\partial x}\right)^2+1}}$ and $\cos\lambda^{\#} = \frac{\sqrt{\left(\frac{\partial h}{\partial x}\right)^2+1}}{\sqrt{\left(\frac{\partial h}{\partial x}\right)^2+\left(\frac{\partial h}{\partial y}\right)^2+1}}$. Using the same method of solving Eq. (A6), we can obtain the basis vectors of the coordinate $[O; \boldsymbol{x}_2, \boldsymbol{y}_2, \boldsymbol{z}_2]$ shown in Fig. A3 as follows:

$$\begin{pmatrix} \boldsymbol{x}_2 \\ \boldsymbol{y}_2 \\ \boldsymbol{z}_2 \end{pmatrix} = \begin{pmatrix} \cos\theta^{\#} & 0 & -\sin\theta^{\#} \\ -\sin\lambda^{\#}\sin\theta^{\#} & \cos\lambda^{\#} & -\sin\lambda^{\#}\cos\theta^{\#} \\ \cos\lambda^{\#}\sin\theta^{\#} & \sin\lambda^{\#} & \cos\lambda^{\#}\cos\theta^{\#} \end{pmatrix} \begin{pmatrix} \boldsymbol{i} \\ \boldsymbol{j} \\ \boldsymbol{k} \end{pmatrix}. \tag{A12}$$

Now, let's summarize the expressions of the basis vectors of the OS coordinate solved by the four kinds of coordinate rotations in Table A1.

GMDD
6, 5801–5862, 2013

Appendix B

Scalars in the OS coordinate

Let the expression of a vector $\boldsymbol{A}$ in the z coordinate and the OS coordinate, respectively, be

$$\boldsymbol{A} = \begin{pmatrix} a & b & c \end{pmatrix} \begin{pmatrix} \boldsymbol{i} \\ \boldsymbol{j} \\ \boldsymbol{k} \end{pmatrix}, \tag{B1}$$

and

$$\boldsymbol{A} = \begin{pmatrix} \alpha & \beta & \gamma \end{pmatrix} \begin{pmatrix} \boldsymbol{i}_o \\ \boldsymbol{j}_o \\ \boldsymbol{k}_o \end{pmatrix}. \tag{B2}$$

where $\boldsymbol{i}$, $\boldsymbol{j}$, and $\boldsymbol{k}$ are the basis vectors of the z coordinate, $\boldsymbol{i}_o$, $\boldsymbol{j}_o$, and $\boldsymbol{k}_o$ are the basis vectors of the OS coordinate, a, b, and c are the scalars of vector $\boldsymbol{A}$ in the z coordinate, and the α, β, and γ are the scalars of vector $\boldsymbol{A}$ in the OS coordinate.

Using the first kind of basis vectors of the OS coordinate as an example, and substituting its expression in Table 3 into Eq. (B2), we obtain

$$\boldsymbol{A} = \begin{pmatrix} \alpha & \beta & \gamma \end{pmatrix} \begin{pmatrix} \cos(b\cdot\lambda) & -\sin(b\cdot\theta)\sin(b\cdot\lambda) & -\cos(b\cdot\theta)\sin(b\cdot\lambda) \\ 0 & \cos(b\cdot\theta) & -\sin(b\cdot\theta) \\ \sin(b\cdot\lambda) & \sin(b\cdot\theta)\cos(b\cdot\lambda) & \cos(b\cdot\theta)\cos(b\cdot\lambda) \end{pmatrix} \begin{pmatrix} \boldsymbol{i} \\ \boldsymbol{j} \\ \boldsymbol{k} \end{pmatrix}. \tag{B3}$$

Comparing Eqs. (B3) and (B1), we obtain

$$\begin{pmatrix} a & b & c \end{pmatrix} = \begin{pmatrix} \alpha & \beta & \gamma \end{pmatrix} \begin{pmatrix} \cos(b\cdot\lambda) & -\sin(b\cdot\theta)\sin(b\cdot\lambda) & -\cos(b\cdot\theta)\sin(b\cdot\lambda) \\ 0 & \cos(b\cdot\theta) & -\sin(b\cdot\theta) \\ \sin(b\cdot\lambda) & \sin(b\cdot\theta)\cos(b\cdot\lambda) & \cos(b\cdot\theta)\cos(b\cdot\lambda) \end{pmatrix}. \tag{B4}$$

GMDD
6, 5801–5862, 2013

Using Eq. (B4), we can solve the scalars α, β, and γ of vector $\boldsymbol{A}$ in the OS coordinate as follows:

$$(\alpha\ \beta\ \gamma) = (a\ b\ c)\begin{pmatrix} \cos(b\cdot\lambda) & -\sin(b\cdot\theta)\sin(b\cdot\lambda) & -\cos(b\cdot\theta)\sin(b\cdot\lambda) \\ 0 & \cos(b\cdot\theta) & -\sin(b\cdot\theta) \\ \sin(b\cdot\lambda) & \sin(b\cdot\theta)\cos(b\cdot\lambda) & \cos(b\cdot\theta)\cos(b\cdot\lambda) \end{pmatrix}^{-1}. \quad \text{(B5)}$$

In conclusion, we can use the transformation matrix of the OS coordinate and the scalar values of a vector in the z coordinate to calculate its scalar values in the OS coordinate.

Appendix C

Parameters and scalars in the unified framework

The values of the three parameters in the unified framework of the z coordinate, the CS coordinate and the OS coordinate are all listed in Table C1. In addition, the equations of the new method proposed by Li et al. (2012) can also be combined in this unified framework, as shown in Table C1.

In order to obtain the scalars of a vector of each coordinate in the unified framework, we use a coordinate transformation matrix $\mathbf{t}_{ij}$ to define these scalars as follows:

$$(\alpha\ \beta\ \gamma) = (a\ b\ c)\begin{pmatrix} t_{11}\ t_{21}\ t_{31} \\ t_{12}\ t_{22}\ t_{32} \\ t_{13}\ t_{23}\ t_{33} \end{pmatrix}^{-1}, \quad \text{(C1)}$$

where α, β, and γ are the scalars in the unified framework, and a, b, and c are the scalars in the z coordinate. Then, via defining the value of the matrix $\mathbf{t}_{ij}$ in each coordinate, we obtain the values of scalars in each coordinate. And the values of $\mathbf{t}_{ij}$ in the z coordinate, the CS coordinate, and the OS coordinate are given as follows:

GMDD
6, 5801–5862, 2013

$\mathbf{t}_{ij}$ in the z coordinate,

$$\mathbf{t}_{ij} = \begin{pmatrix} 1 & 0 & 0 \\ 0 & 1 & 0 \\ 0 & 0 & 1 \end{pmatrix}; \tag{C2}$$

$\mathbf{t}_{ij}$ in the contravariant equations of the CS coordinate,

$$\mathbf{t}_{ij} = \begin{pmatrix} 1 & 0 & \frac{H_t - z}{H_t - h} \cdot \frac{\partial h}{\partial x} \\ 0 & 1 & \frac{H_t - z}{H_t - h} \cdot \frac{\partial h}{\partial y} \\ 0 & 0 & \frac{H_t - h}{H_t} \end{pmatrix}; \tag{C3}$$

$\mathbf{t}_{ij}$ in the covariant equations of the CS coordinate,

$$\mathbf{t}_{ij} = \begin{pmatrix} 1 & 0 & 0 \\ 0 & 1 & 0 \\ \frac{H_t(z-H_t)}{(H_t-h)^2}\frac{\partial h}{\partial x} & \frac{H_t(z-H_t)}{(H_t-h)^2}\frac{\partial h}{\partial y} & \frac{H_t}{H_t-h} \end{pmatrix}; \tag{C4}$$

$\mathbf{t}_{ij}$ in the OS coordinate using the first basis vectors,

$$\mathbf{t}_{ij} = \begin{pmatrix} \cos(b\cdot\lambda) & -\sin(b\cdot\theta)\sin(b\cdot\lambda) & -\cos(b\cdot\theta)\sin(b\cdot\lambda) \\ 0 & \cos(b\cdot\theta) & -\sin(b\cdot\theta) \\ \sin(b\cdot\lambda) & \sin(b\cdot\theta)\cos(b\cdot\lambda) & \cos(b\cdot\theta)\cos(b\cdot\lambda) \end{pmatrix}; \tag{C5}$$

$\mathbf{t}_{ij}$ in the OS coordinate using the second basis vectors,

$$\mathbf{t}_{ij} = \begin{pmatrix} \cos\left(b\cdot\theta'\right) & 0 & \sin\left(b\cdot\theta'\right) \\ -\sin\left(b\cdot\theta'\right)\sin\left(b\cdot\lambda'\right) & \cos\left(b\cdot\lambda'\right) & \cos\left(b\cdot\theta'\right)\sin\left(b\cdot\lambda'\right) \\ -\sin\left(b\cdot\theta'\right)\cos\left(b\cdot\lambda'\right) & -\sin\left(b\cdot\lambda'\right) & \cos\left(b\cdot\theta'\right)\cos\left(b\cdot\lambda'\right) \end{pmatrix}. \tag{C6}$$

GMDD
6, 5801–5862, 2013

Acknowledgements. The comments of the editor helped us to improve the analyses of the advection experiments and the presentation of the whole paper. The first author wishes to acknowledge the helpful discussions about the CFL criterion in the OS coordinate with Hilary Weller, Jinxi Li, Li Dong, and Shiming Xu.

The first and second authors were supported by the Knowledge Innovation Program of the Chinese Academy of Sciences (KZCX2-YW-Q11-04) and the National Basic Research Program of China (973 Program, Grant No. 2011CB309704). The third author was supported by the National Natural Science Foundation of China (NSFC) under Grant No. 41175064.

References

Adcroft, A.: Representation of topography by porous barriers and objective interpolation of topographic data, Ocean Model., 67, 13–27, 2013.

Adcroft, A., Hill, C., and Marshall, J.: Representation of topography by shaved cells in a height coordinate ocean model, Mon. Weather Rev., 125, 2293–2315, 1997.

Adcroft, A., Hallberg, R., and Harrison, M.: A finite volume discretization of the pressure gradient force using analytic integration, Ocean Modell., 22, 106–113, 2008.

Arakawa, A. and Lamb, V. R.: Computational design of the basic dynamical processes of the UCLA general circulation model, Methods in Computational Physics: Advances in Research and Applications, Academic Press, Chang, J., Vol. 17, 173–265, 1977.

Berntsen, J.: A perfectly balanced method for estimating the internal pressure gradients in σ coordinate ocean models, Ocean Modell., 38, 85–95, 2011.

Bleck, R.: An oceanic general circulation model framed in hybrid isophycnic-Cartesian coordinates, Ocean Modell., 37, 55–88, 2002.

Blumberg, A. F. and Mellor, G. L.: A description of a three-dimensional coastal ocean circulation model. Three-dimensional coastal ocean models, American Geophysical Union, Heaps, N. S., 1–16, 1987.

Bradley, M. E. and Dowling, T. E.: Using 3-D finite volume for the pressure-gradient force in atmospheric models, Q. J. Roy. Meteor. Soc., 138, 2126–2135, 2012.

Corby, G. A., Gilchrist, A., and Newson, R. L.: A general circulation model of the atmosphere suitable for long period integrations, Q. J. Roy. Meteor. Soc., 98, 809–832, 1972.

GMDD

6, 5801–5862, 2013

Davies, T., Cullen, M. J. P., Malcolm, A. J., Mawson, M. H., Staniforth, A., White, A. A., and Wood, N.: A new dynamical core for the Met Office's global and regional modelling of the atmosphere, Q. J. Roy. Meteor. Soc., 131, 1759–1782, 2005.

Gal-Chen, T. and Somerville, R. C. J.: On the use of a coordinate transformation for the solution of the Navier–Stokes Equations, J. Comput. Phys., 17, 209–228, 1975.

Gary, J. M.: Estimate of truncation error in transformed coordinate, primitive equation atmospheric models, J. Atmos. Sci., 30, 223–233, 1973.

Haney, R. L.: On the pressure gradient force over steep topography in sigma coordinate ocean models, J. Phys. Oceanogr., 21, 610–619, 1991.

Janjić, Z.: Pressure gradient force and advection scheme used for forecasting with steep and small scale topography, Contrib. Atmos. Phys., 50, 186–199, 1977.

Ji, L., Chen, J., Zhang, D., and Wang, H.: Review of some numerical aspects of the dynamic framework of NWP model, Chin. J. Atoms. Sci., 29, 120–130, 2005 (in Chinese).

Konor, C. S. and Arakawa, A.: Design of an atmospheric model based on a generalized vertical coordinate, Mon. Weather Rev., 125, 1649–1673, 1997.

Klemp, J. B.: A terrain-following coordinate with smoothed coordinate surfaces, Mon. Weather Rev., 139, 2163–2169, 2011.

Klemp, J. B.: Experiences with a smoothed terrain-following vertical coordinate in MPAS, Multiscale numerics for the atmosphere and ocean, Cambridge, UK, 3 October 2012.

Leuenberger, D., Koller, M., Fuhrer, O., and Schär, C.: A generelization of the SLEVE vertical coordinate, Mon. Weather Rev., 138, 3683–3689, 2010.

Li, Y., Wang, B., and Wang, D.: Characteristics of terrain-following sigma coordinate, Atmos. Oceanic Sci. Lett., 4, 157–161, 2011.

Li, Y., Wang, D., and Wang, B.: A new approach to implement sigma coordinate in a numerical model, Commun. Comput. Phys., 12, 1033–1050, 2012.

Lin, S.: A finite-volume integration method for computing pressure gradient force in general vertical coordinates, Q. J. Roy. Meteor. Soc., 123, 1749–1762, 1997.

Madec, G.: Nemo Ocean Engine, Note du Pôle de Modélisation, Institut Pierre-Simon Laplace (IPSL), France, No 27, ISSN No 1288–1619, 2008.

Mesinger, F.: On the convergence and error problems of the calculation of the pressure gradient force in sigma co-ordinate models, Geophys. Astrophys. Fluid Dyn., 19, 105–117, 1982.

GMDD
6, 5801–5862, 2013

Mesinger, F., Chou, S.-C., Gomes, J. L., Jovic, D., Bastos, P., Bustamante, J. F., Lazic, L., Lyra, A. A., Morelli, S., Ristic, I., and Veljovic, K.: An upgraded version of the eta model, Meteorol. Atmos. Phys., 116, 63–79, 2012.

Phillips, N. A.: A coordinate system having some special advantages for numerical forecasting, J. Meteorol., 14, 184–185, 1957.

Qian, Y. and Zhong, Z.: General forms of dynamic equations for atmosphere in numerical models with topography, Adv. Atmos. Sci., 3, 10–22, 1986.

Sangster, W. E.: A method of representing the horizontal pressure force without reduction of station pressures to sea level, J. Meteorol., 17, 166–176, 1960.

Schär, C., Leuenberger, D., Fuhrer, O., Lüthi, D., and Girard, C.: A new terrain-following vertical coordinate formulation for atmospheric prediction models, Mon. Weather Rev., 130, 2459–2480, 2002.

Schättler, U., Doms, G., and Schraff, C.: A description of the nonhydrostatic regional COSMO-model part VII: user's guide, available at: http://www.cosmo-model.org/content/model/documentation/core/cosmoUserGuide.pdf (last access: 25 September 2013), 2012.

Siddorn, J. R. and Furner, R.: An analytical stretching function that combines the best attributes of geopotential and terrain-following vertical coordinates, Ocean Modell., 66, 1–13, 2013.

Sikirić, M. D., Janeković, I., and Kuzmić, M.: A new approach to bathmetry smoothing in σ coordinate ocean models, Ocean Modell., 29, 128–136, 2009.

Simmons, A. J. and Burridge, D. M.: An energy and angular-momentum conserving vertical finite-difference scheme and hybrid vertical coordinates, Mon. Weather Rev., 109, 758–766, 1981.

Simmons, A. J. and Strüfing, R.: Numerical forecasts of stratospheric warming events using a model with a hybrid vertical coordinate, Quart. J. Roy. Meteor. Soc., 109, 81–111, 1983.

Skamarock, W. C., Klemp, J. B., Dudhia, J., Gill, D. O., Barker, D. M., Duda, M. G., Huang, X.-Y., Wang, W., and Powers, J. G.: A description of the advanced research WRF Version 3, NCAR Tech. Note NCAR/TN-475+STR, 113 pp., 2008.

Skamarock, W. C., Klemp, J. B., Duda, M. G., Fowler, L. D., Park, S.-H., and Ringler, T.: A multi Scale nonhydrostatic atmospheric model using centroidal Voronoi tesselations and C-grid staggering, Mon. Weather Rev., 140, 3090–3105, 2012.

Smagorinsky, J., Strickler, R. F., Sangster, W. E., Manabe, S., Halloway Jr., J. L., and Hembree, G. D.: Prediction experiments with a general circulation model, in: Proc. Int. Symp. on Dynamics of Large Scale Atmospheric Processes, Moscow, USSR, 70–134, 1967.

GMDD
6, 5801–5862, 2013

Steppeler, J., Hess, R., Schattler, U., and Bonaventura, L.: Review of numerical methods for nonhydrostatic weather prediction models, Meteorol. Atmos. Phys., 82, 287–301, 2003.
Steppeler, J., Park, S.-H., and Dobler, A.: Forecasts covering one month using a cut-cell model, Geosci. Model Dev., 6, 875–882, doi:10.5194/gmd-6-875-2013, 2013.
Sundquist, H.: On truncation errors in sigma-system models, Atmosphere, 13, 81–95, 1975.
Sundquist, H.: On vertical interpolation and truncation in connection with use of sigma-system models, Atmosphere, 14, 37–52, 1976.
Wallcraft, A. J., Metzger, E. J., and Carroll, S. N.: Software design description for the Hybrid coordinate ocean model (HYCOM) version 2.2. NRL/MR/7320–09-9166, 149 pp., 2009.
Wang, B., Wan, H., Ji, Z., Zhang, X., Yu, R., Yu, Y., and Liu, H.: Design of a new dynamical core for global atmospheric models based on some efficient numerical methods, Sci. China, Ser. A, 47, Supp. 4–21, 2004.
Yamazaki, H. and Satomura, T.: Nonhydrostatic atmospheric modeling using a combined Cartesian grid, Mon. Weather Rev., 138, 3932–3945, 2010.
Yu, R.: Design of the limited area numerical weather prediction model with steep mountains, Chin. J. Atoms. Sci., 13, 145–158, 1989.
Zängl, G.: An improved method for computing horizontal diffusion in a sigma-coordinate model and its application to simulation over mountainous topography, Mon. Weather Rev., 130, 1423–1432, 2002.
Zängl, G.: A generalized sigma-coordinate system for the MM5, Mon. Weather Rev., 131, 2875–2884, 2003.

GMDD
6, 5801–5862, 2013

Table 1. Principles of the basis vectors and coordinates of the OS coordinate.

Values of each coordinate		Basis vectors
Vertical	Horizontal	
Keeping Constant at the surface of terrain and the top of model		The two horizontal basis vectors are in the tangent plane of the terrain
Equaling to height z, when there is no terrain	Equaling to x or y, when there is no terrain	Orthogonal to each other

GMDD
6, 5801–5862, 2013

Table 2. Two kinds of rotated basis vectors after the 3-D rotation.

Two kinds of basis vectors	Expressions
The first kind	$\boldsymbol{i}_o = \boldsymbol{i}\cos\lambda - \boldsymbol{j}\sin\theta\cdot\sin\lambda - \boldsymbol{k}\cos\theta\cdot\sin\lambda$ $\boldsymbol{j}_o = \boldsymbol{j}\cos\theta - \boldsymbol{k}\sin\theta$ $\boldsymbol{k}_o = \boldsymbol{i}\sin\lambda + \boldsymbol{j}\sin\theta\cdot\cos\lambda + \boldsymbol{k}\cos\theta\cdot\cos\lambda$
The second kind	$\boldsymbol{i}_o = \boldsymbol{i}\cos\theta' + \boldsymbol{k}\sin\theta'$ $\boldsymbol{j}_o = -\boldsymbol{i}\sin\theta'\cdot\sin\lambda' + \boldsymbol{j}\cos\lambda' + \boldsymbol{k}\cos\theta'\cdot\sin\lambda'$ $\boldsymbol{k}_o = -\boldsymbol{i}\sin\theta'\cdot\cos\lambda' - \boldsymbol{j}\sin\lambda' + \boldsymbol{k}\cos\theta'\cdot\cos\lambda'$

GMDD
6, 5801–5862, 2013

Table 3. Basis vectors of the OS coordinate.

Two kinds of basis vectors	Expressions
The first kind	$\boldsymbol{i}_o = \boldsymbol{i}\cos(b\cdot\lambda) - \boldsymbol{j}\sin(b\cdot\theta)\cdot\sin(b\cdot\lambda) - k\cos(b\cdot\theta)\cdot\sin(b\cdot\lambda)$ $\boldsymbol{j}_o = \boldsymbol{j}\cos(b\cdot\theta) - \boldsymbol{k}\sin(b\cdot\theta)$ $\boldsymbol{k}_o = \boldsymbol{i}\sin(b\cdot\lambda) + \boldsymbol{j}\sin(b\cdot\theta)\cdot\cos(b\cdot\lambda) + \boldsymbol{k}\cos(b\cdot\theta)\cdot\cos(b\cdot\lambda)$
The second kind	$\boldsymbol{i}_o = \boldsymbol{i}\cos(b\cdot\theta') + \boldsymbol{k}\cdot\sin(b\cdot\theta')$ $\boldsymbol{j}_o = -\boldsymbol{i}\sin(b\cdot\theta')\cdot\sin(b\cdot\lambda') + \boldsymbol{j}\cos(b\cdot\lambda') + \boldsymbol{k}\cos(b\cdot\theta')\cdot\sin(b\cdot\lambda')$ $\boldsymbol{k}_o = -\boldsymbol{i}\sin(b\cdot\theta')\cdot\cos(b\cdot\lambda') - \boldsymbol{j}\sin(b\cdot\lambda') + \boldsymbol{k}\cos(b\cdot\theta')\cdot\cos(b\cdot\lambda')$

GMDD
6, 5801–5862, 2013

Table 4. The horizontal and vertical spatial resolutions of all the sensitive experiments.

Fixed resolution (horizontal or vertical) (units: m)	Variable resolution (horizontal or vertical) (units: m)	The corresponding horizontal or vertical grid number
dZ = 0.5, with the vertical grid number being 50	dX = 0.5	600
	dX = 1.0*	300
	dX = 2.0	150
	dX = 4.0	75
	dX = 8.0	37
dX = 1.0, with the horizontal grid number being 300	dZ = 0.25	100
	dZ = 0.5*	50
	dZ = 1.0	25
	dZ = 2.0	12
	dZ = 4.0	6

* These groups have been implemented in the basic comparison in Sect. 4.2.

GMDD
6, 5801–5862, 2013

Table A1. Expressions of the basis vectors of the OS coordinate after four kinds of coordinate rotations.

Ways of the rotation	Expression of the basis vectors
First: on the upslope of terrain, around the x axis and then the rotated y axis	$\boldsymbol{i}_o = \boldsymbol{i}\cos\lambda^* - \boldsymbol{j}\sin\theta^*\cdot\sin\lambda^* + \boldsymbol{k}\cos\theta^*\cdot\sin\lambda^*$ $\boldsymbol{j}_o = \boldsymbol{j}\cos\theta^* + \boldsymbol{k}\sin\theta^*$ $\boldsymbol{k}_o = -\boldsymbol{i}\sin\lambda^* - \boldsymbol{j}\sin\theta^*\cdot\cos\lambda^* + \boldsymbol{k}\cos\theta^*\cdot\cos\lambda^*$
Second: on the upslope of terrain, around the y axis and then the rotated x axis	$\boldsymbol{i}_o = \boldsymbol{i}\cos\theta' + \boldsymbol{k}\sin\theta'$ $\boldsymbol{j}_o = -\boldsymbol{i}\sin\theta'\cdot\sin\lambda' + \boldsymbol{j}\cos\lambda' + \boldsymbol{k}\cos\theta'\cdot\sin\lambda'$ $\boldsymbol{k}_o = -\boldsymbol{i}\sin\theta'\cdot\cos\lambda' - \boldsymbol{j}\sin\lambda' + \boldsymbol{k}\cos\theta'\cdot\cos\lambda'$
Third: on the downslope of terrain, around the x axis and then the rotated y axis	$\boldsymbol{i}_o = \boldsymbol{i}\cos\lambda - \boldsymbol{j}\sin\theta\cdot\sin\lambda - \boldsymbol{k}\cos\theta\cdot\sin\lambda$ $\boldsymbol{j}_o = \boldsymbol{j}\cos\theta - \boldsymbol{k}\sin\theta$ $\boldsymbol{k}_o = \boldsymbol{i}\sin\lambda + \boldsymbol{j}\sin\theta\cdot\cos\lambda + \boldsymbol{k}\cos\theta\cdot\cos\lambda$
Fourth: on the downslope of terrain, around the y axis and then the rotated x axis	$\boldsymbol{i}_o = \boldsymbol{i}\cos\theta^\# - \boldsymbol{k}\sin\theta^\#$ $\boldsymbol{j}_o = -\boldsymbol{i}\sin\theta^\#\cdot\sin\lambda^\# + \boldsymbol{j}\cos\lambda^\# - \boldsymbol{k}\cos\theta^\#\cdot\sin\lambda^\#$ $\boldsymbol{k}_o = \boldsymbol{i}\sin\theta^\#\cdot\cos\lambda^\# + \boldsymbol{j}\sin\lambda^\# + \boldsymbol{k}\cos\theta^\#\cdot\cos\lambda^\#$

GMDD
6, 5801–5862, 2013

Table C1. Values of all the parameters in the unified framework.

Parameters	Values			
	z coordinate	CS coordinate		OS coordinate
		Contravariant equations	Covariant equations (Li et al., 2012)	
λ_{1m}	$\lambda_{11}=0$	$\lambda_{11}=0$	$\lambda_{11}=-\frac{1}{2}v^m v^n \frac{\partial g_{nm}}{\partial q^1}$	$\lambda_{11}=0$
	$\lambda_{12}=0$	$\lambda_{12}=0$	$\lambda_{12}=-\frac{1}{2}v^m v^n \frac{\partial g_{nm}}{\partial q^2}$	$\lambda_{12}=0$
	$\lambda_{13}=0$	$\lambda_{13}=0$	$\lambda_{13}=-\frac{1}{2}v^m v^n \frac{\partial g_{nm}}{\partial q^3}$	$\lambda_{13}=0$
λ_2	$\lambda_2=1$	$\lambda_2=\sqrt{g}=\sqrt{\lvert \mathbf{g}_{ij} \rvert}$		$\lambda_2=1$
δ_{mi}	$\delta_{mi}=\begin{pmatrix}1&0&0\\0&1&0\\0&0&1\end{pmatrix}$	$\delta_{mi}=\mathbf{g}^{ij}$	$\delta_{mi}=\begin{pmatrix}1&0&0\\0&1&0\\0&0&1\end{pmatrix}$	$\delta_{mi}=\begin{pmatrix}1&0&0\\0&1&0\\0&0&1\end{pmatrix}$

GMDD
6, 5801–5862, 2013

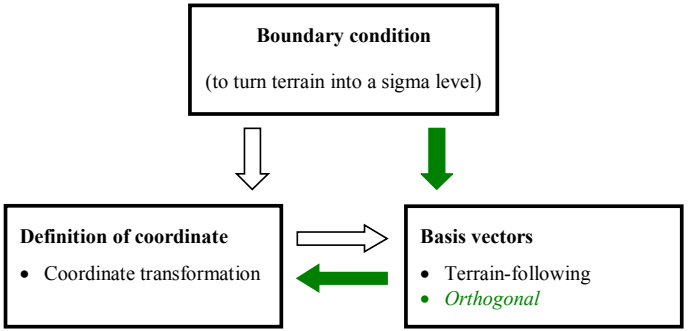

Fig. 1. Design of the OS coordinate. The green arrows are for the OS coordinate, and the black arrows, the CS coordinate.

GMDD
6, 5801–5862, 2013

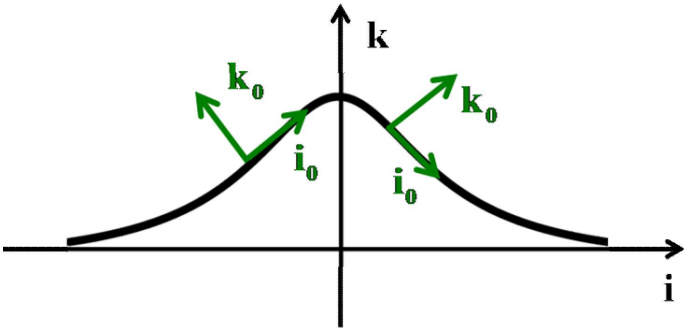

Fig. 2. A 2-D schematic of the coordinate rotation. The black curve is the terrain, the black arrows are the basis vectors of the z coordinate, and the green arrows are the rotated basis vectors.

GMDD
6, 5801–5862, 2013

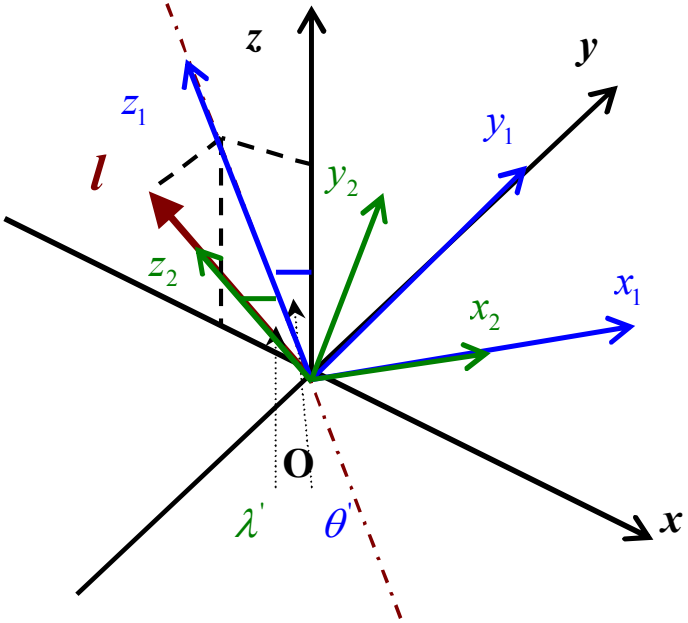

Fig. 3. Schematic 3-D rotation for solving the basis vectors of the OS coordinate on the upslope of the terrain. The burgundy arrow is the normal vector of the terrain, and the burgundy dash-dotted line is its projection on the plane *Oxz*. The black arrows are the basis vectors of the *z* coordinate, the blue arrows are the basis vectors of the first rotated coordinate $[O; \boldsymbol{x}_1, \boldsymbol{y}_1, z_1]$, and the green arrows are the basis vectors of the second rotated coordinate $[O; \boldsymbol{x}_2, \boldsymbol{y}_2, z_2]$.

GMDD
6, 5801–5862, 2013

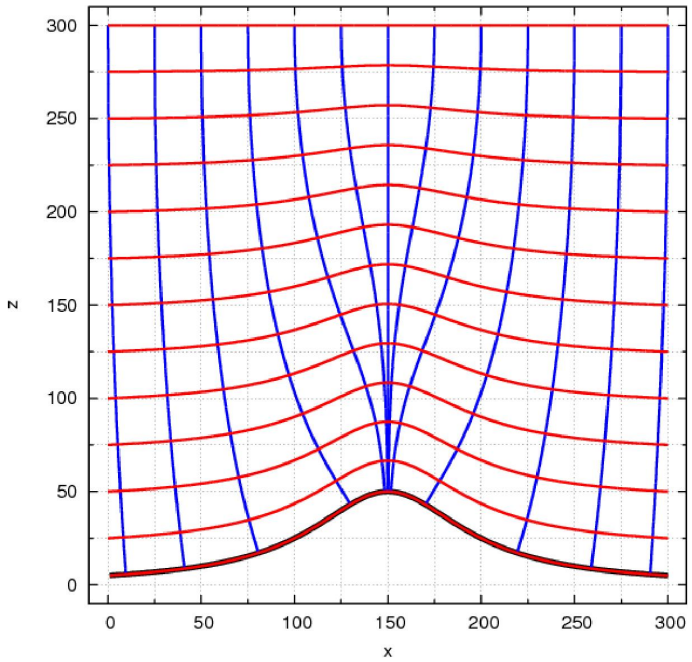

Fig. 4. The grid of the OS coordinate. The red lines are the σ coordinate, and the blue lines are the x' coordinate, and the black curve represents the terrain.

GMDD
6, 5801–5862, 2013

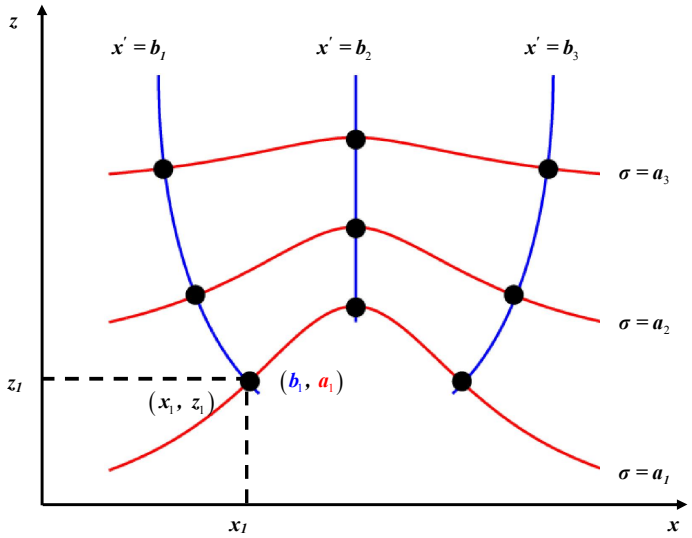

Fig. 5. Schematic of the coordinate transformation between the z coordinate and the OS coordinate using the "cross-point way." The blue curves are the x' coordinate, the red curves are the σ coordinate, and the black dots mark where they cross each other. The x and z axis represent the horizontal and vertical direction of the z coordinate, respectively.

GMDD
6, 5801–5862, 2013

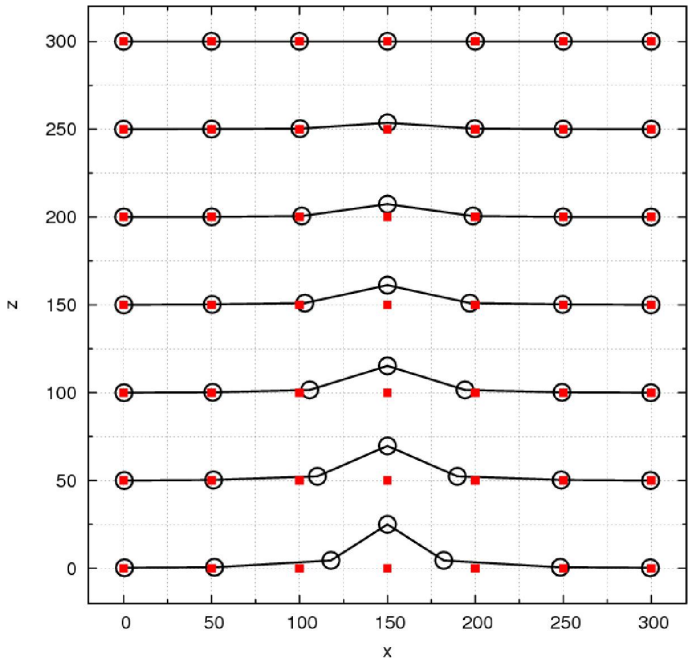

Fig. 6. Transformation between the z coordinate and the OS coordinate. The solid red squares are for the OS coordinate, and the open black circles are for the z coordinate.

GMDD
6, 5801–5862, 2013

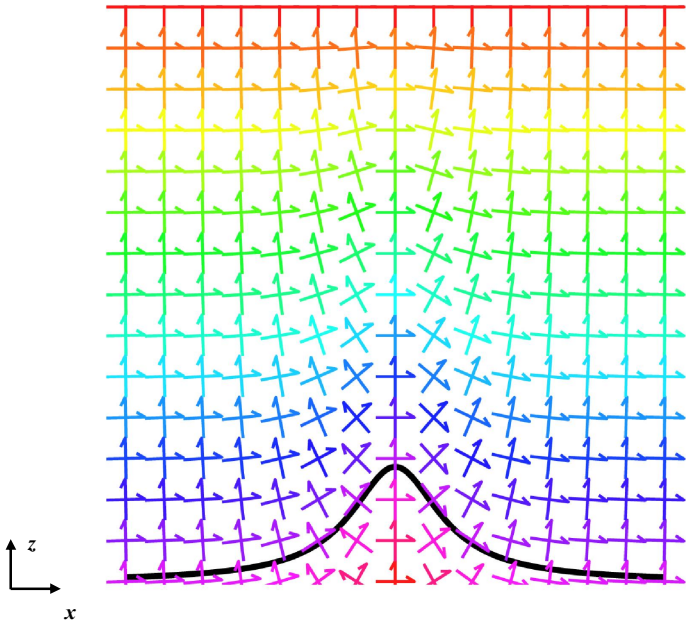

Fig. 7. The vertical pattern of the basis vectors of the OS coordinate. The black curve represents the terrain, and the colored arrows are the basis vectors of the OS coordinate. Different colors are used for the basis vectors at different σ levels.

GMDD
6, 5801–5862, 2013

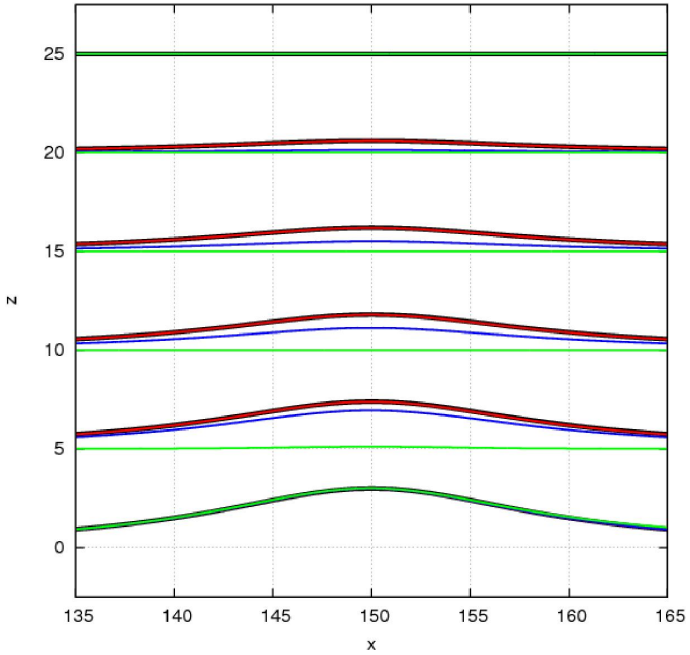

Fig. 8. The σ levels in the OS coordinate with different rotation parameterizations of b and those in the CS coordinate. The black lines are the σ levels in the CS coordinate; the red, blue, and green lines are those in the OS coordinate with rotation parameters given by Eqs. (34)–(36), respectively.

GMDD
6, 5801–5862, 2013

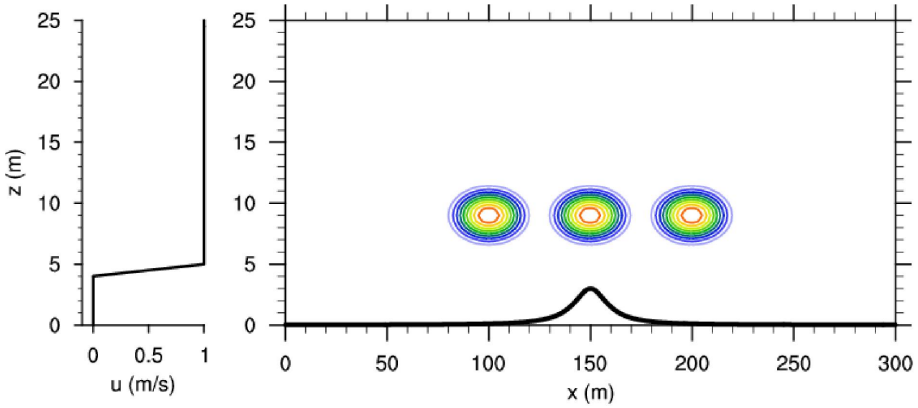

Fig. 9. Parameters used in the 2-D linear advection experiments. The left panel is the vertical profile of the *u* field. The colored contours in the right panel represent the anomaly field *q* with the contour interval of 0.1, and the thick black curve, the terrain.

GMDD
6, 5801–5862, 2013

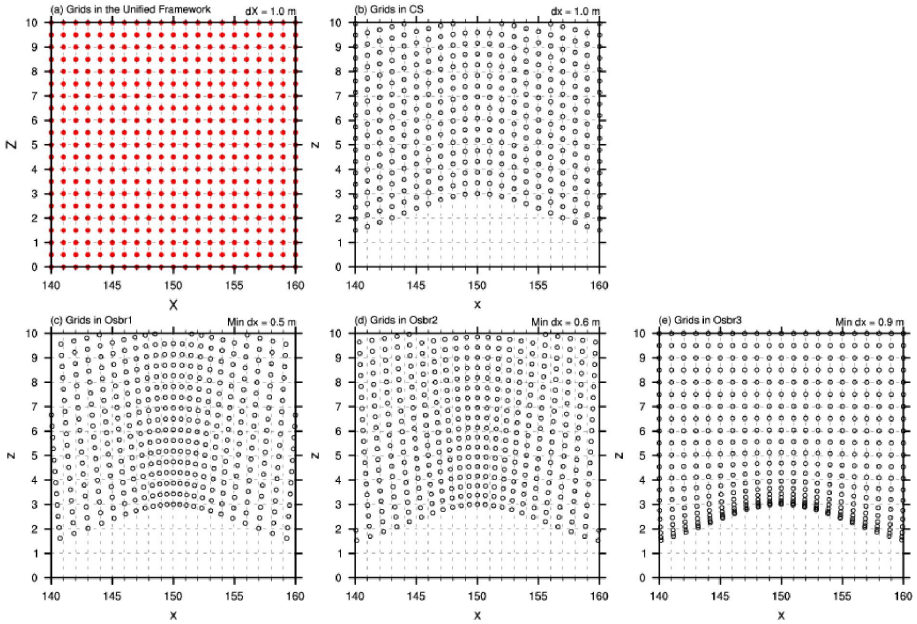

Fig. 10. Computational grids above the top of terrain in the CS coordinate and the OS coordinate with three different rotation parameter *b*. The solid red dots in **(a)** are the grids in the view of the transformed space, and the open black circles in **(b–e)** are the grids in the view of the physical space.

GMDD
6, 5801–5862, 2013

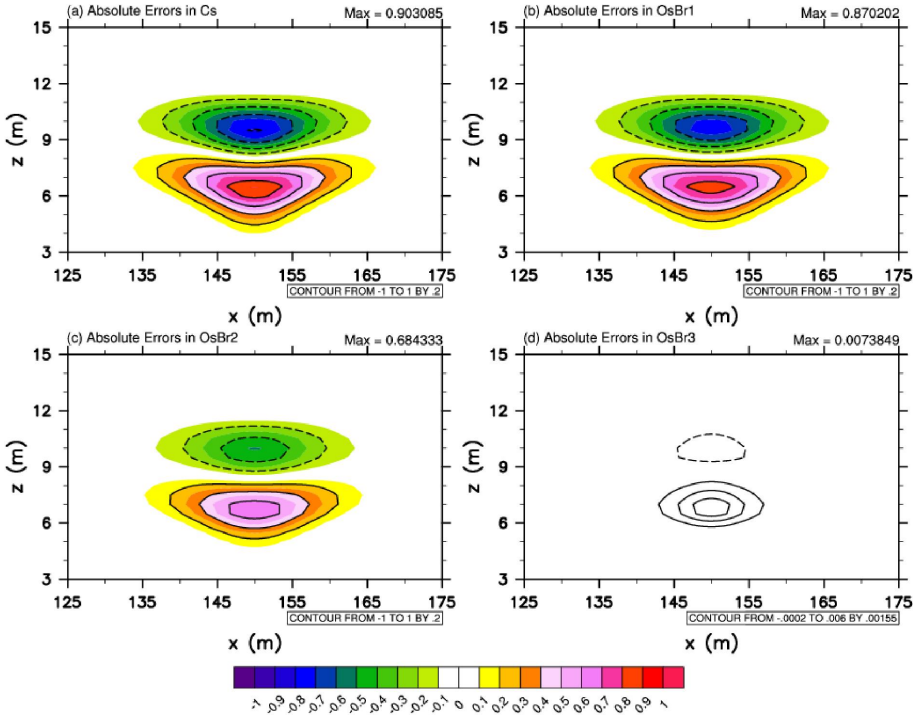

Fig. 11. Absolute errors of the CS coordinate and the OS coordinate with three different rotation parameters of b compared with the non-terrain simulation, when the advection is over the top of the terrain (t = 200 s). Shading represents the AE. The solid black contours are for positive values, and the dashed contours are for negative values. The contour interval is 0.2 in **(a–c)**; the contours in **(d)** are −0.0002, 0.002, 0.004, and 0.006.

GMDD
6, 5801–5862, 2013

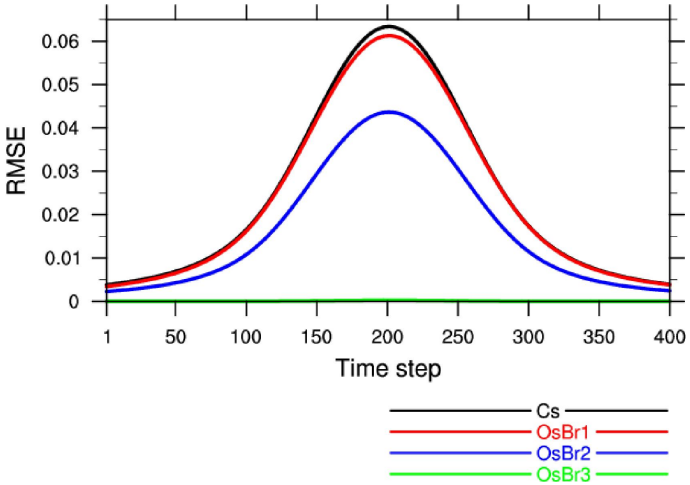

Fig. 12. RMSEs of all four experiments with respect to the non-terrain simulation at every time step.

GMDD
6, 5801–5862, 2013

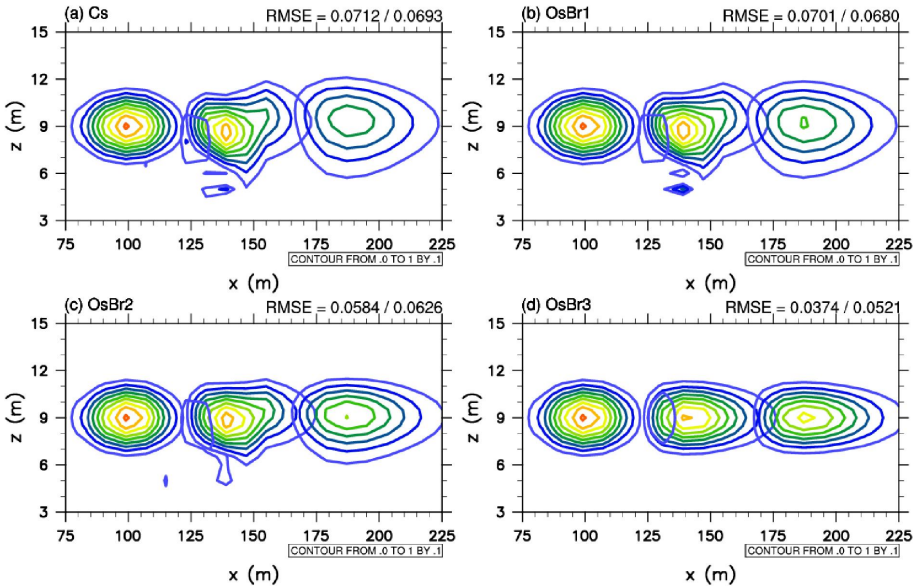

Fig. 13. The advection at the beginning (t = 0 s), the middle (t = 200 s), and the end (t = 400 s) of the integration in the experiment of dX = 8.0 m and dZ = 0.5 m. Colored contours are the anomaly field q, with the contour interval of 0.1.

GMDD
6, 5801–5862, 2013

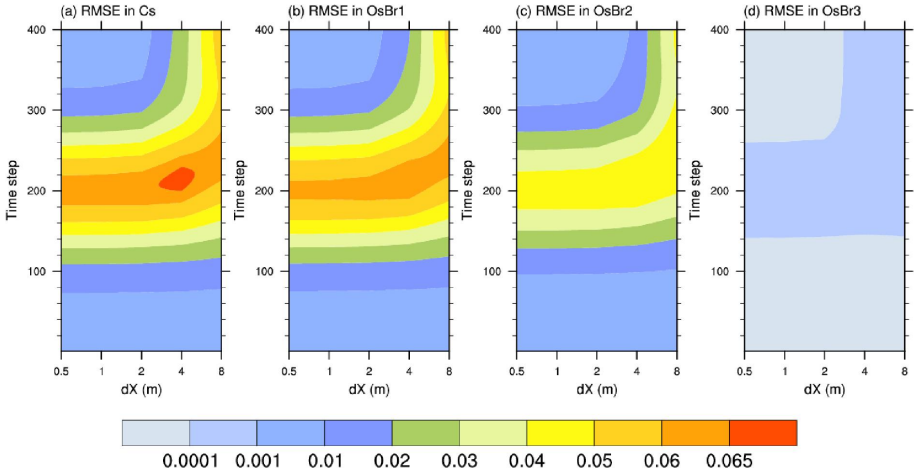

Fig. 14. RMSEs of all the sensitive experiments using five different horizontal spatial resolutions with respect to the non-terrain simulation at every time step. The left one is the result obtained using the CS coordinate, and the other three are the results obtained using the OS coordinate with linear, squared, and exponential rotation parameters of *b*, respectively.

GMDD
6, 5801–5862, 2013

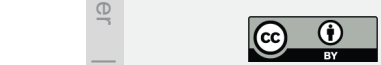

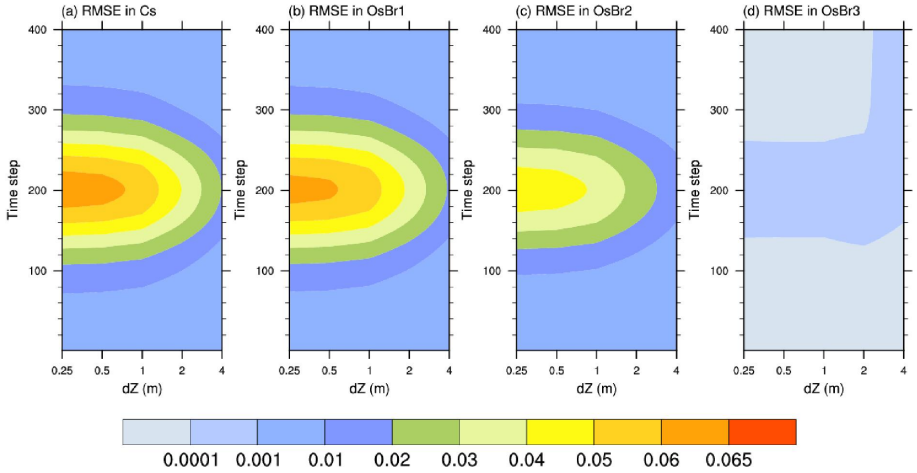

Fig. 15. Same as Fig. 14, except for the RMSEs obtained using five different vertical spatial resolutions.

GMDD
6, 5801–5862, 2013

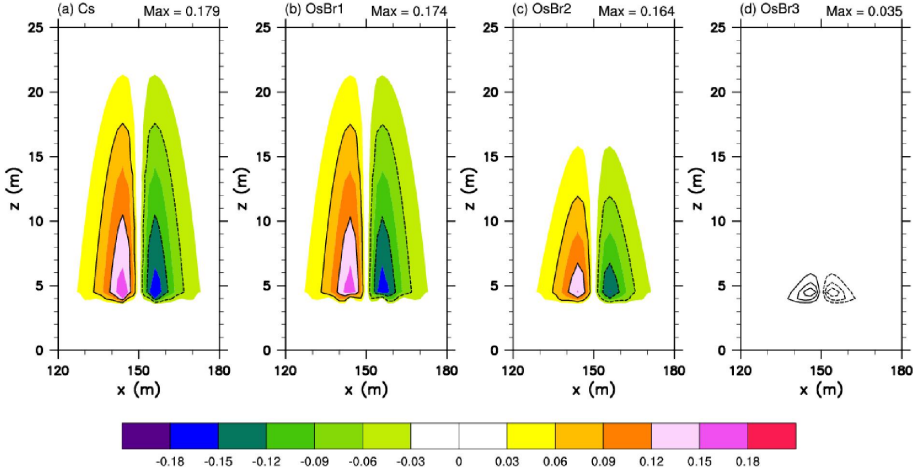

Fig. 16. Slopes of every σ levels above 4 m over the top of terrain in the CS coordinate and the OS coordinate using three kinds of rotation parameter b in the experiment of dX = 2.0 m and dZ = 0.5 m. The shadings are the slopes. The solid black contours are for positive values, and the dashed contours are for negative values. The contour interval in **(a–c)** is 0.06, but that in **(d)** is 0.006.

GMDD
6, 5801–5862, 2013

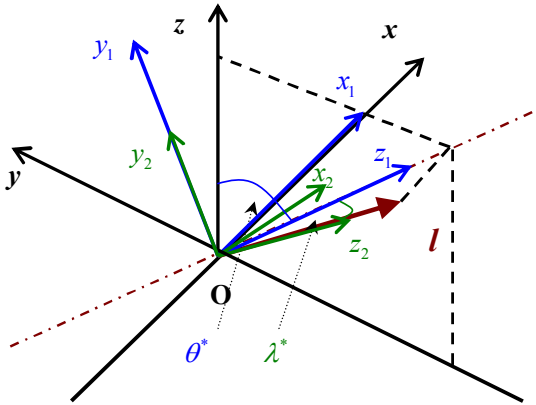

Fig. A1. Schematic 3-D rotation for solving the basis vectors of the OS coordinate on the upslope of the terrain. The burgundy arrow is the normal vector of the terrain, and the burgundy dash-dotted line is its projection on the plane *Oyz*. The black arrows are the basis vectors of the *z* coordinate, the blue arrows are the basis vectors of the first rotated coordinate $[O; \boldsymbol{x}_1, \boldsymbol{y}_1, z_1]$, and the green arrows are the basis vectors of the second rotated coordinate $[O; \boldsymbol{x}_2, \boldsymbol{y}_2, z_2]$.

GMDD
6, 5801–5862, 2013

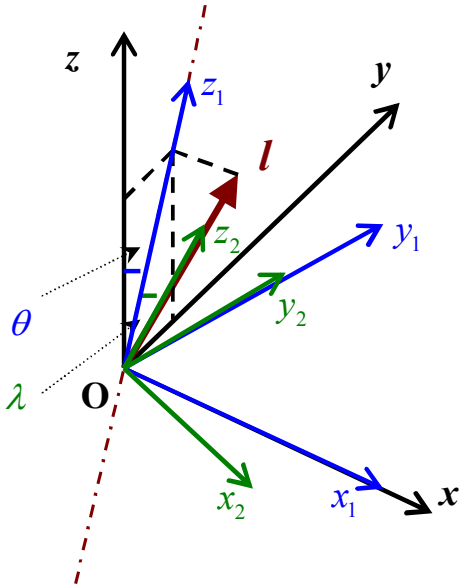

Fig. A2. Same as Fig. A1, except that the rotation is on the downslope of the terrain and the first rotation is around the *x* axis and then the rotated *y* axis. The burgundy dash-dotted line is the projection of the normal vector of terrain on the plane *Oyz.*

GMDD
6, 5801–5862, 2013

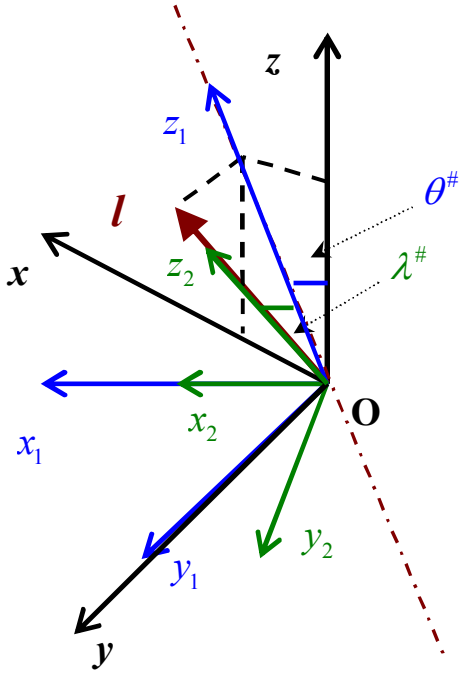

Fig. A3. Same as Fig. A1, except the rotation is on the downslope of the terrain and the first rotation is around the *y* axis and then the rotated *x* axis. The burgundy dash-dotted line is the projection of the normal vector of terrain on the plane *Oxz*.

GMDD
6, 5801–5862, 2013